UNIVERSITÀ DI PISA

Dipartimento di Oncologia, dei Trapianti
e delle Nuove Tecnologie in Medicina
Corso di Dottorato in Tecnologie per la Salute:
Valutazione e Gestione delle Innovazioni nel Settore Biomedicale
X9 Ciclo

Ph.D Thesis

Image guided robotic assistance for the diagnosis and treatment of tumor

Cinzia Freschi

Submitted to the University of Pisa in partial fulfillment
of the requirements for the degree of Doctor of Philosophy

Tutor:

Prof. Andrea Pietrabissa

Prof. Mauro Ferrari

Dr. Vincenzo Ferrari

It was defended on February 2011

Table of contents

Abstract

The aim of this thesis is to demonstrate the feasibility and the potentiality of introduction of robotics and image guidance in the overall oncologic workflow, from the diagnosis to the treatment phase.

The popularity of robotics in the operating room has grown in recent years. Currently the most popular systems is the da Vinci telemanipulator (Intuitive Surgical), it is based on a master-slave control, for minimally invasive surgery and it is used in several surgical fields such us urology, general, gynecology, cardiothoracic. An accurate study of this system, from a technological field of view, has been conducted addressing all drawbacks and advantages of this system. The da Vinci System creates an immersive operating environment for the surgeon by providing both high quality stereo visualization and a human-machine interface that directly connects the surgeon's hands to the motion of the surgical tool tips inside the patient's body. It has undoubted advantages for the surgeon work and for the patient health, at least for some interventions, while its very high costs leaves many doubts on its price benefit ratio.

In the robotic surgery field many researchers are working on the optimization and miniaturization robots mechanic, while others are trying to obtain smart functionalities to realize robotic systems, that, "knowing" the patient anatomy from radiological images, can assists the surgeon in an active way.

Regarding the second point, image guided systems can be useful to plan and to control medical robots motion and to provide the surgeon pre-operative and intra-operative images with augmented reality visualization to enhance his/her perceptual capacities and, as a consequence, to improve the quality of treatments.

To demonstrate this thesis some prototypes has been designed, implemented and tested.

The development of image guided medical devices, comprehensive of augmented reality, virtual navigation and robotic surgical features, requires to address several problems. The first ones are the choosing of the robotic platform and of the image source to employ.

An industrial anthropomorphic arm has been used as testing platform. The idea of integrating industrial robot components in the clinical workflow has been supported by the da Vinci technical analysis.

The algorithms and methods developed, regarding in particular robot calibration, based on literature theories and on an easily integration in the clinical scenario, can be adapted to each anthropomorphic arm. In this way this work can be integrated with light-weight robots, for industrial or clinical use, able to work in close contact to humans, which will become numerous in the early future.

Regarding the medical image source, it has been decided to work with ultrasound imaging. Two-dimensional ultrasound imaging is widely used in clinical practice because is not dangerous for the patient, inexpensive, compact and it is a highly flexible imaging that allows users to study many anatomic structures. It is routinely used for diagnosis and as guidance in percutaneous treatments. However the use of 2D ultrasound imaging presents some disadvantages that require great ability of the user: it requires that the clinician mentally integrates many images to reconstruct a complete idea of the anatomy in 3D. Furthermore the freehand control of the probe make it difficult to individuate anatomic positions and orientations and probe repositioning to reach a particular location. To overcome these problems it has been developed an image guided system that fuse 2D US real time images with routinely CT or MRI 3D images, previously acquired from the patient, to enhance clinician orientation and probe guidance.

The implemented algorithms for robot calibration and US image guidance has been used to realize two applications responding to specific clinical needs. The first one to speed up the execution of routinely and very recurrently procedures like percutaneous biopsy or ablation. The second one to improve a new completely non invasive type of treatment for solid tumors, the HIFU (High Intensity Focused Ultrasound).

An ultrasound guided robotic system has been developed to assist the clinician to execute complicated biopsies, or percutaneous ablations, in particular for deep abdominal organs. It was developed an integrated system that provides the clinician two types of assistance: a mixed reality visualization allows accurate and easy planning of needle trajectory and target reaching verification; the robot arm equipped with a six-degree-of-freedom force sensor allows the precise positioning of the needle holder and allows the clinician to adjust, by means of a cooperative control, the planned trajectory to overcome needle deflection and target motion.

The second application consists in an augmented reality navigation system for HIFU treatment. HIFU represents a completely non invasive method for treatment of solid tumors, hemostasis and other vascular features in human tissues. The technology for HIFU treatments is still evolving and the systems available on the market have some limitations and drawbacks. A disadvantage resulting from our experience with the machinery available in our hospital (JC200 therapeutic system Haifu (HIFU) by Tech Co., Ltd, Chongqing), which is similar to other analogous machines, is the long time required to perform the procedure due to the difficulty to find the target, using the remote motion of an ultrasound probe under the patient. This problem has been addressed developing an augmented reality navigation system to enhance US guidance during HIFU treatments allowing an easy target localization. The system was implemented using an additional free hand ultrasound

probe coupled with a localizer and CT fused imaging. It offers a simple and an economic solution to an easy HIFU target localization.

This thesis demonstrates the utility and usability of robots for diagnosis and treatment of the tumor, in particular the combination of automatic positioning and cooperative control allows the surgeon and the robot to work in synergy. Further the work demonstrates the feasibility and the potentiality of the use of a mixed reality navigation system to facilitate the target localization and consequently to reduce the times of sittings, to increase the number of possible diagnosis/treatments and to decrease the risk of potential errors. The proposed solutions for the integration of robotics and image guidance in the overall oncologic workflow, take into account current available technologies, traditional clinical procedures and cost minimization.

Part I – Introduction

1 Context of thesis

Computer science and technology have strongly transformed the clinical practice over the last decades. This technically oriented evolution was parallel to evolutions of medicine[1]. Diagnostic and therapeutic procedures tend to be less invasive for the patient aiming at reducing pain, post-operative complications, and recovery time. Minimal invasiveness results in smaller targets reached through narrow access (natural or not) with no direct sensing (vision, touch) and limited degrees of freedom imposed by the access ports. Main clinical applications are in endoscopic surgery where instruments and optics are introduced in the patient's body through small incisions. it imposes significant ergonomic restriction on the operating surgeon practicing this technique [2] as the surgeon has to overcome the following perceptual-motor difficulties:

• Two dimensional (2D) vision from a conventional monitor (reduces perception of depth);

• A disturbed eye hand-target axis (decreases ergonomics and dexterity);

• Instrument guidance (requires ambidextrous manual activity);

• Long rigid instruments used in laparoscopic surgery (magnify the surgeon's natural hand tremor);

• The instruments have only five degrees of freedom (DOF): four for positioning of the tip and one for the actuation (these limit the surgeon's natural range of motion, decreasing dexterity);

• Fixed abdominal entry points (limit the workspace reachable with the instruments tip);

- Instrument tip and handle move in opposite direction (a technical drawback known as the fulcrum effect and which decreases the motor-perception capability);

- Camera instability (contributes to surgeon fatigue);

- Limited tactile feedback (reduces dexterity).

Further than surgery, all minimally invasive diagnostic or therapeutic procedures require particular ability of the physician.

To overcome to these limitations have been adopted new computer based technologies. Computer assisted surgery (CAS), Computer Assisted Medical Interventions (CAMI), Computer Integrated Surgery and Therapy (CIST) , Image Guided Surgery (IGS), Augmented Reality in Medicine and Surgery, Surgical Navigation, Medical Robotics for Surgery, and others, are different acronyms or expressions that represent the same concept:"Computer assisted surgery aims at providing tools that allow the clinician to use multi-modality data in a rational and quantitative way in order to plan, to simulate and to accurately and safely execute mini-invasive medical interventions"[1].

Medical interventions include both diagnostic and therapeutic actions. Therapy may involve surgery, radiotherapy, local injection of drugs, interventional radiology, etc.

Image guidance, in general, can reduce the inherent invasiveness of surgery and improve localization and targeting by intraoperative imaging using fluoroscopy, ultrasound, magnetic resonance imaging, etc. Alternatively, by means of localization systems, intraoperative image guidance can be based on previously acquired images using reference frames attached to the patient (frame based stereotaxy) or images which are registered to the patient (frameless stereotaxy). In the latter case, computers can pilot the operator through 3D coordinates and thus fulfill the need for enhanced visibility during interventional radiology and minimally invasive surgical procedures.

Furthermore, the fusion of pre-operative and intra-operative data (consisting in medical images and sensors data) in a multimodal representation of the surgical scenario, coherent with the real one, allows the use of programmable (and sometimes intelligent) machines, such as robots and mechatronic tools, that automatically or semi-automatically perform single steps or whole surgical procedures.

An Computer Assisted Surgery (CAS) system then provide two main types of assistance exist: image guidance and robotic aids. In the following paragraph a detailed description of this features is provided.

1.1 Robotic surgical assistance

Robots were first utilized in surgery in the mid 1980s. They used to assist surgeons during neurosurgical and orthopedic procedures, these early surgical devices were designed to aid with predefined tasks that required a high degree of accuracy and reproducibility.

Automation is not a primary goal of medical robotics where the interaction with the clinical operator has to be considered with a very special attention. Indeed, often medical robots are not intended to replace the operator but rather to assist him/her where his/her capabilities are limited. Medical robots may be classified in many ways: by manipulator design (e.g., type of kinematics, type of actuation, …); by automation level (e.g., preprogrammed control versus teleoperated control versus constrained cooperative control), by targeted anatomy or technique (e.g., cardiac, intravascular, percutaneous, laparoscopic, microsurgical); intended operating environment [e.g., in-scanner, conventional operating room (OR)], etc[2]. In this thesis it was chosen to classify robots in base of level of autonomy. Surgical robots assist surgeons for the moving of surgical instruments, sensors, or other devices useful to threat the patient. The type and the level of assistance offered by robots can be classified as follow:

Preprogrammed, semi autonomous motion: The desired behavior of the robot's tools is specified interactively by the surgeon, usually based on medical images. The computer fills in the details and obtains the surgeon's concurrence before the robot is moved. Examples include the selection of needle target and insertion points for percutaneous therapy and tool cutter paths for orthopedic bone machining. An example is the Neuromate system (Integrated Surgical systems, Sacramento, CA) designed to facilitate stereotactic neurosurgical procedures

Teleoperated control: The surgeon specifies the desired motions directly through a separate human interface device and the robot moves immediately its arms as required. Examples include common telesurgery system such as the da Vinci. Although physical master manipulators are the most common input devices, other human interface are also used, i.e voice control (Aesop by Intuitive Surgical, Inc).

Cooperative control: The surgeon can grasps tool held by the robot or a control handle on the robot's end effector. Often force sensors sense the direction that the surgeon wishes to impose on the tool and the controller moves the robot as desired. Early experiences showed that the surgeons found this form of control to be very convenient and natural for surgical tasks.

These control modes are not mutually exclusive and are frequently mixed. For example, the Robodoc system (Integrated Surgical Systems, Inc. of Sacramento, California), a robot for orthopedic surgery, uses cooperative control to position the robot close the patient's femur or knee and then preprogrammed motions for bone machining are executed. Similarly the LARS robot [3] used cooperative and teleoperated control modes always in the field of orthopedic surgery.

The popularity of robotics in the operating room has grown in recent years. Currently the most popular systems is the da Vinci telemanipulator (Intuitive Surgical) used in several surgical fields such

us urology, general, gynecological cardiothoracic. This technology has undoubted advantages for the surgeon but it is very bulky and expensive. Despite the large number of reported series and randomized controlled clinical trials the evidence of benefit from use of this very expensive technology remains uncertain. Even if exist many clinical studies and also some economic evaluation to try to quantify robot efficacy in respect to its cost, until now no detailed studies describing it from a technological point of view are done. In the thesis an accurate review of the da Vinci from an engineering point of view was performed and it is shown in the next part.

1.2 Image Guidance

In the field of minimal invasive image guided surgery, images from modalities like CT, MRI and ultrasound are used to plan a surgical procedure, to guide the surgeon intraoperatively to move surgical instruments a to monitor the procedure and to control and evaluate the results. The first computer-assisted systems that tried to bridge the gap between preoperative diagnostic image data (CT, MRI) and the patient in the operating room were used in the neurological field and were frame-based stereotactic systems [4-6]. These systems used specially designed frames, attached to the patient's head during preoperative image acquisition and surgery, in order to register the images to the patient. Though highly accurate these systems had several disadvantages (invasive, cumbersome and time-consuming) and were gradually replaced by frame-less stereotactic systems [6-7] as improvement of the technology. The actual image guided systems differ in the way they integrate preoperative image data with physical space (i.e. patient registration), the kind of tracking technology they use to follow the surgical tools that are used (e.g. optical, magnetic, ultrasonic or mechanical) and in the way the image information is presented to the surgeon. A short overview of the major components of an image guided system is given.

3D model generation and Visualization: The first step is the acquisition of preoperative medical images of the target anatomy. Given a volume dataset, usually from magnetic resonance imaging (MRI) or computed tomography (CT), it can be necessary either to reconstruct a 3D digital model of the information contained (to be used in further processing), or to render images representing the same information. There are two basic classes of volume visualization algorithms in use today: Surface–based Rendering techniques and Direct Volume Rendering techniques (Fig. 1-1). In volume rendering, images are created directly from the volume data, and no intermediate geometry is extracted. The key idea of surface-based rendering methods is to extract intermediate surface descriptions (by means of a segmentation process) of the relevant objects from the volume data, which are in general produced and stored as triangle meshes, then used for rendering. The general approach used to perform the surface extraction after dataset segmentation is called "marching cube". An important point is that the intermediate result (the 3D surface-based digital model) can be used for many other applications, such as the computation of volumes or masses, the creation of physical copies, an easier integration with physical models (e.g. for the representation of deformable materials), etc. The importance of surface-based techniques is thus not restricted to pure visualization.
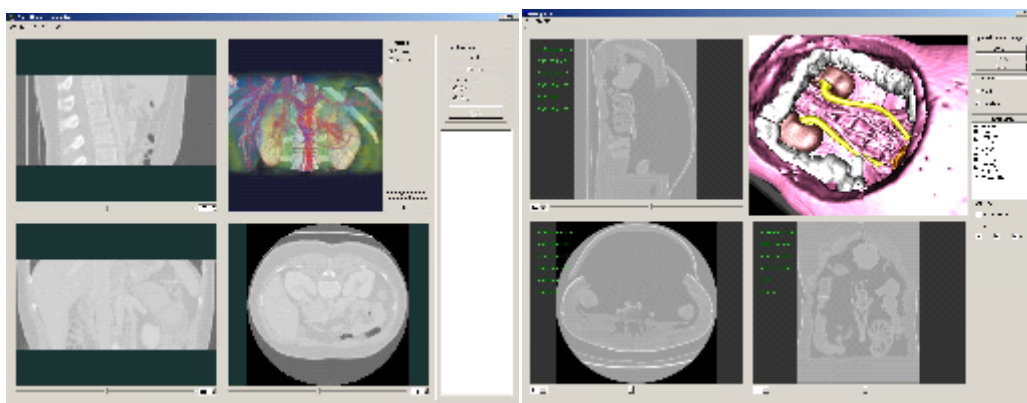

Fig. 1-1 Example of 3D Visualization with volume (a) and surface rendering(b)

Localization and Calibration of surgical tools. Intra-operatively, a localizer system (usually optical or electromagnetic) is used to allow the localization and tracking of position and orientation of tools (surgical instruments, therapeutic or imaging devices and robotic system). Localization of tools requires their sensorization and calibration. Sensors have to be designed and positioned in order to guaranty their functionality and safety. Calibration procedure is required to determine the relation between the sensor and the tool. Often image guided systems integrate a 3D model of each tool to show its real time position. Calibration allows to calculate where the tool 3D model have to be positioned in respect to the position and the orientation read from the sensor.

Patient Registration. Mixing virtual pre-operative information (extracted from the medical dataset) with real intraoperative information (consisting in the patient himself), requires the alignment of the virtual anatomy to the real one. This process, called registration, requires to determine the geometrical transformation of correspondent points taken in two different reference frames and in two different time instants. In fact, pre-operative information are given in the reference frame of the radiological device and are acquired some days before the intervention, while the intra-operative information are given in the reference frame of surgical room (defined by means of a tracking system) and are acquired during the intervention the patient's anatomy to the 3D patient model obtained preoperatively.

Image guided systems based on preoperative images have a serious disadvantage. During the surgical procedure, the anatomy move and deform so that images acquired before surgery (i.e. the map) will not correspond to the patient any more.

The anatomy shift problem [8-9] can only be solved adequately by integrating intraoperative imaging with navigation technology. A common way of doing this is to transport the patient in and out of an

intraoperative CT [10-12] or MRI [13-15] scanner in order to update the images (i.e. the map) during surgery (the scanners can also be moved over the patient). This has obvious logistic drawbacks that limit the practical number of 3D scans acquired during surgery. Interventional MRI systems [16-18] solve these problems by the surgeon have to operate inside the magnet. Further, these systems require high investments, high running costs, and a special operating room broader as well as surgical equipment. Intraoperative ultrasound [19-20] is a flexible, relatively low costs alternative that has gained a increasing acceptance as a result of improved image quality and integration with navigation technology. However, 2D a 3D ultrasound acquisition covers only a limited part of the surgical field making it hard to get an overview of surrounding anatomy, which frequently is needed. In addition, high quality preoperative CT and MRI data are often generated anyway for diagnostic and planning purposes and additional functional MRI will often be beneficial, both for preoperative planning and guidance. Hence in order to perform safe and accurate surgery it will be beneficial to use intraoperative ultrasound in combination with preoperative MRI / CT. There are different strategies for the combined use of both pre and intraoperative data. Indirect use of ultrasound to track the anatomical changes that occur, apply these changes to elastically modify preoperative data and navigate according to manipulated MRI/CT volumes have been suggested.

In the present work ultrasound data are used as maps for intraoperative navigation and preoperative data are used for procedure planning, and to provide an overview of the anatomy during image guided interventions.

1.3 Contribution of the thesis

The work has been done at the EndoCAS Center, Cisanello Hospital, Pisa (Italy). One of the main activity of the center is the development of high-tech systems designed to overcome the current limits of surgery

and radiology. EndoCAS carry out simultaneously basic and applied research. Starting from real clinical problems and defining the technical-functional specifications for an "ideal" system that can solve them, the center faces the basic research issues to find the solution necessary to develop the system. In the opposite direction, the results of basic research at the state of the art are pushed into the design of new Computer assisted systems in order to improve the current surgical procedures, to reduce their invasiveness, or to allow new interventional procedures. It was developed a generic platform for computer assisted surgery presented in the next paragraph. The solutions developed in this thesis were integrated and used in the EndoCAS Navigator platform. In other cases EndoCAS Navigator was used as testing environment because, integrating several aspects of CAS into a modular open architecture, allows rapid developing of new functionalities and new applications [21-23]. The dissertation often refers to EndoCAS Navigator platform and its components.

1.3.1 EndoCAS Navigator

From a functional point of view, the specifics of the platform are illustrated in Fig. 1-2(left).
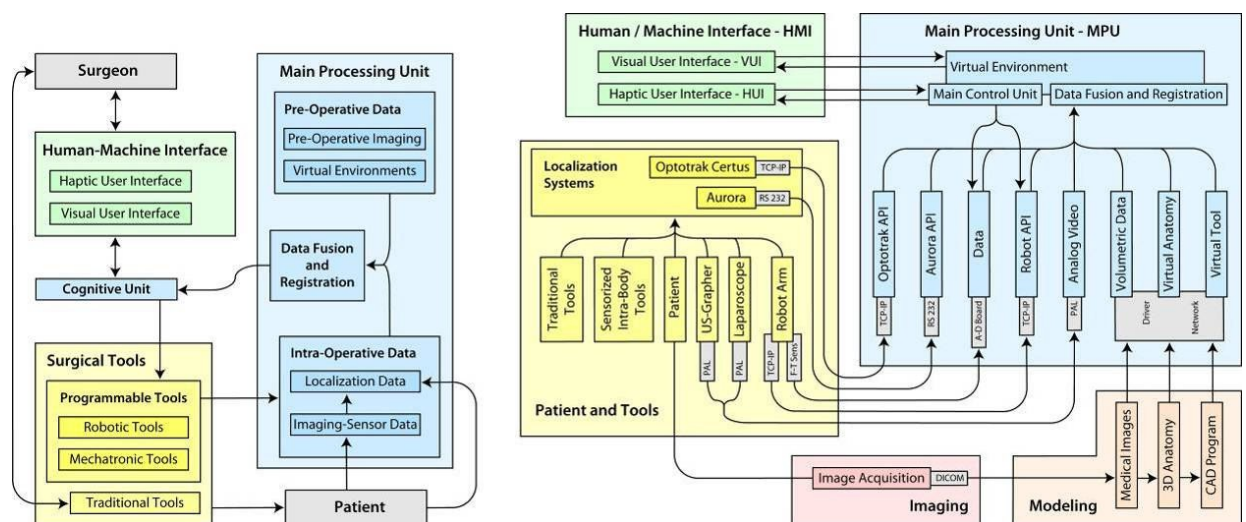

Fig. 1-2 The functional scheme of the computer assistance system (left) and scheme of the integrated CAS system, showing the hardware and software components, the architecture and the intercommunication (right)

The scheme highlights the communication between the main functional modules of the system and the interaction between system, surgeon and patient. The platform consists of three main functional modules: the surgical tools, the main processing unit, and the human/machine interface. The surgical tools module comprises the instruments used to perform the interventions. Tools are classified into traditional tools and programmable tools. Tools commonly used in surgical practice and managed by surgeon in a traditional way fall in the first category. These tools, used for imaging (laparoscopes, ultrasound probes, etc.) and intervention (scalpel, forceps, cauterizer, drill, biopsy needle, etc.), are passive, for what concerns movement control, and work under direct manual control of the surgeon. In contrast, programmable tools category encompasses active, intelligent tools (such as mechatronic and robotic tools), provided with sensors and programmable actuation capabilities. The main processing unit (MPU) processes and integrates preoperative data with intraoperative data concerning the surgical environment and the internal status of the programmable tools. Integrated data (provided by the Data Fusion and Registration module) are processed by the Cognitive Unit and returned to the surgeon in form of sensorial enhancement by means of the Human/Machine Interface (HMI). The HMI is composed by two modules that can function independently: the Visual User Interface (VUI) and the Haptic User Interface (HUI). The status of both interfaces is updated in real-time. The surgeon interacts with the programmable tools through the HMI. The Cognitive Unit, integrating commands given on the HMI with the information provided by the MPU, provides for visual safe guidance and monitoring dangerous situations that may occur during navigation (i.e. contact, proximity etc.) and acts as an intelligent and active filter to the programmable tools commands given by the surgeon, inhibiting or re-interpreting the most critical ones. The synergy between system and surgeon is achieved by means of the Cognitive Unit which by implementing a closed loop between surgeon's commands, programmable tools and MPU, enhances overall performance. EndoCAS

Navigator is based on the described functional approach, and enables the selection of the appropriate components for specific applications. The system can be used for preoperative visualization, diagnosis and planning, intra-operative passive and active guidance. Furthermore, the system integrates components such that it is capable of adaptation for a variety of application domains. The integrated system is illustrated in Fig. 1-2 (right), which highlights the hardware and software components and their intercommunication. The availability of virtual models of all relevant elements in the surgical scene is a prerequisite for the construction of the Virtual Environment. Medical images of the patient are acquired preoperatively (Image Acquisition). Surface models are created by a modeling process in order to build realistic geometrical virtual models of the anatomical organs and structures (Virtual Anatomy) involved in the intended operation. Virtual models of the surgical tools (Virtual Tools) and of all devices that will interact with the patient are generated using computer aided design programs. During the intervention, in order to place the elements correctly in the surgical scene, realtime information about their spatial position are provided by the localizer. The different reference frames, in which spatial coordinates are described, need to be co-registered and aligned with the virtual representations of the anatomies (registration).The geometrical description of the surgical scene is enhanced by information derived from intraoperative imaging devices (Laparoscope, US) and data collected by different types of sensors. All these data sets are integrated into the virtual environment by a Data Fusion process. Both optical (Optotrak Certus®, Northern Digital Inc.) and electromagnetic (NDI Aurora®, Northern Digital Inc.) localization devices have been integrated in the platform respectively for external-body and internal-body localization. A software module, on the top of API of the localizers, that provides a unique interface to configuration and management functions, and allows the use of both in the same application, has been developed and integrated. The module also implements methods for calibration of localization sensors with respect to tools shape and

17

functionalities. Specific procedures have been implemented for automatic dynamic calibration of sensors mounted on the surgical tools, and for manual calibration based on the digitalization of reference points on the tools. Other calibration procedures concern the robot-localizer calibration, and intra-operative imaging devices calibration (such us laparoscopic camera and US probe). The control loop implemented in the core of the MPU (Cognitive Unit) monitors the virtual environment and is responsible for determining the feedback actions associated to the state of the virtual environment. Virtual environments are created integrating in the same view both extracted surfaces and original volumetric datasets (orthogonal slices). The visualization module (developed using the open source framework OpenSG [www.opensg.org]) allows the visualization of virtual environments, modification of the virtual scene settings (transparency, slice position, organs to be visualized), virtual navigation inside the patient by moving the viewpoint by means of a 6D mouse, and perception of stereoscopic images by means of a Head Mounted Display (HMD). Also mixed-reality functionalities have been integrated. The module implements two main functions: the video acquisition and streaming function that manages the image capture from a generic local or remote video source, and the mixing function that synthesizes the hybrid image using video frames and virtual 3D models.
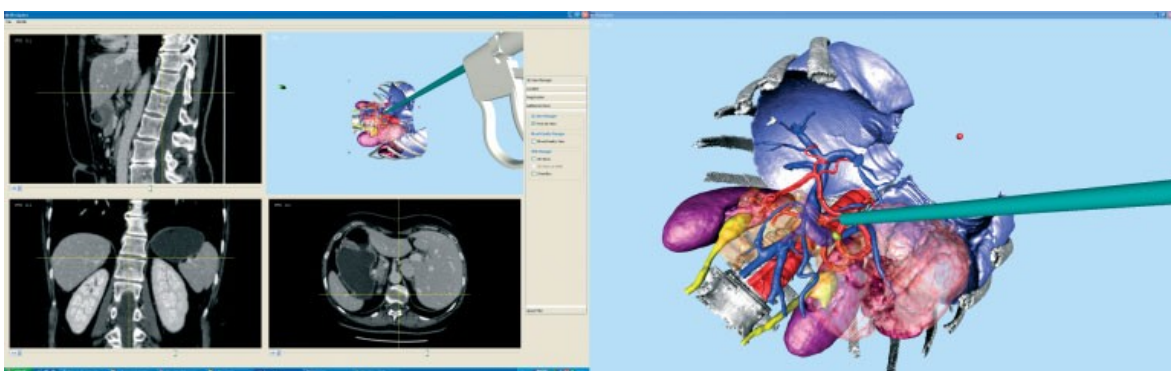

Fig. 1-3 GUI and virtual scenario of the EndoCAS laparoscopy navigator

In the platform has been integrated an industrial robot to provide active surgical assistance and accurate positioning during intervention (chapter 3).

1.3.2 Structure of the thesis

The following part of the thesis describes the operative work performed. In the chapter 2 the review of the daVinci from an engineering point of view is presented. In the chapters 3 and 4 are addressed the two main issues the integration of a robot (chapter 3) and of an ultrasound imaging system (chapter 4) in a image guided system. In the chapter 5 are presented two application implemented an ultrasound robotic guided biopsy and an mixed reality navigation system for HIFU treatment. Finally in Part III the conclusions are drawn.

Part II Work Description

2 The da Vinci robot from an engineering point of view

During the thesis it has been made an accurate review of the literature regarding da Vinci surgical tele-manipulator from an engineering technical view point [24]. The description done in the following pages allows to understand what are the technical aspects that determine robot advantages and motivations of its (few) drawbacks.

The review is based on publications identified in a detailed literature search on ISI Web and PubMed databases and on scrutiny of design details described in patents submitted by Intuitive Surgical Inc. in addition to other relevant papers not indexed on ISI Web or in PubMed but identified from the indexed papers. Additionally, where appropriate in order to understand or clarify some aspects of the robot some key exercises have been performed directly with the da Vinci, available at our institution in Pisa.

Da Vinci System Description

The da Vinci is a teleoperating robotic system based on a master-slave control. It consists of two major subsystems. One subsystem is the surgeon's console, housing the image display, the surgeon's master interfaces, the surgeon's user interface and the electronic controller. The second subsystem is the patient side cart, consisting of the slave manipulators: fully sterilizable surgical instruments and tool robotic arms. Additionally, the sterilizable camera is attached to third robotic arm and is mechanically identical to the others, except for a dedicated camera attachment.

The daVinci System creates an immersive operating environment for the surgeon by providing both high quality stereo visualization and a man-machine interface that directly connects the surgeon's hands to

the motion of the surgical tool tips inside the patient's body. The surgeon visualizes the stereoscopic images by a 3D display located above the hands, restoring hand-eye coordination and providing an intuitive correspondence with manipulations. Furthermore, the controller transforms the spatial motion of the instruments into the camera frame of reference, so that the surgeon feels as if his hands are inside the patient's body. Lastly, the da Vinci system restores the degrees of freedom lost in conventional laparoscopy by placing a 3 DOF wrist inside the patient enabling natural wrist pronation/supination, and providing a total of seven DOF for control of the instrument tip (3 orientation, 3 translation and grip). The system also uses its control system to filter out surgeon tremor, making the instrument tips steadier compared to the unassisted hand. Also, the system allows for variable motion scaling from each master (moved by surgeon's hands) to each slave.

Design description and movement of surgical instruments

From a functional viewpoint, the system offers two features: surgical scenario visualization, by means of the laparoscope connected to the 3D display and transformations of the surgeon's hands movements to the movements of the surgical instruments. Since the first version (in 2000 the robot received FDA approval) the system has been modified, however the master console and the slave robot mechanisms have essentially remained the same (the changes made relate only to their mechanical design).

Patient side cart

Fig. 2-1 Da Vinci patient side chart.

The cart (Fig. 2-1) consists of a moveable base with 4 mounted arms: one for endoscope/camera placement and three for instrument manipulation. All four arms are attached to a central column through vertical prismatic joints. Each of the arms has a set of non-actuated joints (adjusted manually by releasing the associated brakes) that position a distal set of active joints (controlled by the surgeon through the master surgical tools – these can also be adjusted manually). The active joints are the only ones that move the end-effectors during surgery, i.e., involved in the performance of the manipulator. All the arms have the same kinematic structure: six non-actuated joints, six active joints and several passive joints (Fig. 2-2) [25].
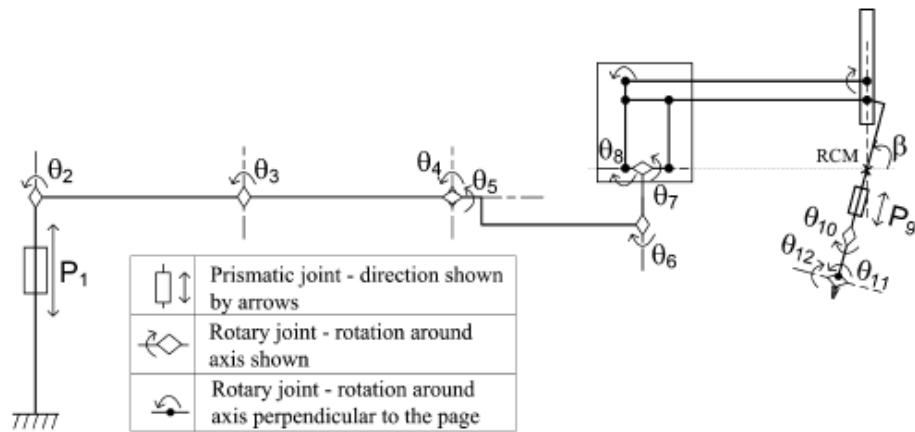
Fig. 2-2 Kinematic configuration of each da Vinci arm consisting of a mechanical chain of links and joints. The symbol ⊥ , on the left, represents the floor of the room where the cart is positioned. Prismatic joints, indicated by Pi, represent links that can translate in respect to the previous one. Rotary joints, indicated with Θi, represent links that can rotate in respect to the previous one. The rotary angle indicated with β represents the remote center of motion (RCM) fixed with the entry point on patient skin.

The last two joints, θ_{11}, θ_{12}, are related to the Endowrist^{TM} instrument tip mechanism (Fig. 2-3), which permit the increased DOF with respect to traditional laparoscopy [26]. The roll around the instrument shaft is represented by θ_{10}. These DOFs are integrated in the da Vinci sterilizable surgical instruments, which can integrate one additional DOF: opening/closing, in case of scissors or grippers.

Fig. 2-3 Detail of a microsurgical EndowristTM instrument: round tip scissors.

The da Vinci surgical instruments are mounted on rail that allows its translation (insertion/extraction into and from the patient's body cavity): P_9.

23

The passive joints indicated with bold dots in Fig. 2-4, form a double parallelogram, that creates a remote centre of motion (RCM). This mechanically constrained kinematic structure ensures that no translational motion occurs against the entry point.
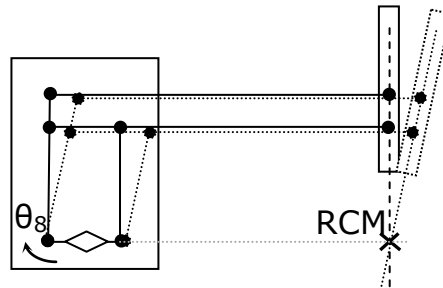

Fig. 2-4 Double parallelogram forming the RCM . Actuation of θ8 joint moves the instrument shaft around RCM.

The robot moves the pitch of the instrument's shaft by moving the entire arm supporting the rail actuating the parallelogram (θ_8). Θ_7 moves the jaws of the instrument's shaft rotating the entire remote centre of motion mechanism. The other joints (passive or servo assisted) are manually moved at the beginning of the intervention to adjust the position of the arms and the fulcrum point. During the intervention they are usually locked.

Surgeon's console

Fig. 2-5 The surgeon at the console and the patient side cart (on the background).

The surgeon controls the slave seated on a stool at the computer console which is positioned remotely from the patient (Fig. 2-5). The console serves as the interface between the surgeon and surgical robot.

The surgeon views the operation through binoculars housed in the console's hood. An infrared beam deactivates the robotic tower whenever the surgeon removes his eyes from the binoculars. The surgeon's arms are supported by a padded armrest. The surgeon can also control motion scaling between movements of the masters and the translated motions of the robotic surgical instruments. The surgeon's console includes two master interfaces, consisting in two kinematics chains movable by the surgeon's hands, which control the two active slave manipulators. The same master interfaces are used together to control camera positioning. This function is activated by a foot pedal.

Fig. 2-6 shows the da Vinci handle. The thumb and index finger of each hand are placed in a virtual gripper interface, attached to each handle of the distal part of the master interface, by means of adjustable Velcro straps.

Fig. 2-6 The da Vinci handle used to remotely move the instruments tip.

Each handle allows rotations around the three Cartesian axes of a frame fixed on the handle itself, by means of sensors. Each handle allows rotations around the three Cartesian axes of a frame fixed on the handle itself, by means of sensors. The handle has a redundant joint (joint number four) as shown in Fig. 2-7.
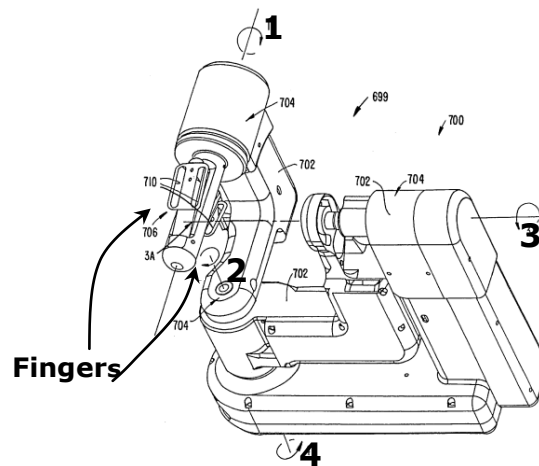
Fig. 2-7 Design details of the da Vinci handle (Patent US6364888B1). The virtual gripper interface, moved by the fingers, allows rotation of the four sensorized joints shown in the figure.

The 4th axis (see axis 4 in the Fig. 2-7) was introduced to permit angles multiples of 180° [Patent US6364888B1].

The handle is attached to the proximal part of the master interface as shown in Fig. 2-8.
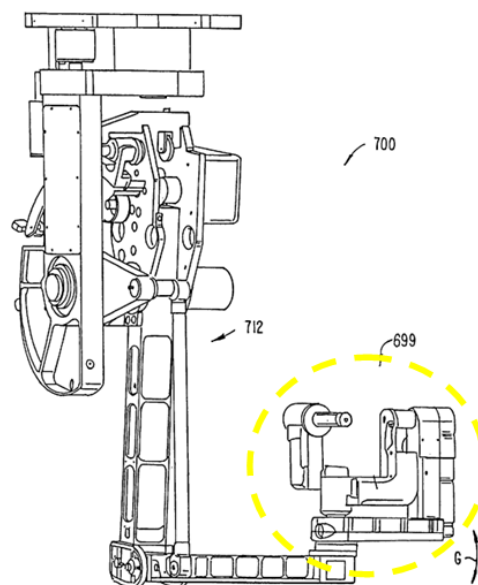

Fig. 2-8 The da Vinci master interface (Patent US6364888B1) with the handle in the yellow circle.

The proximal part of the master interface has three joint that allow the rotations around axes *A*, *B* and *C* (Fig. 2-9).
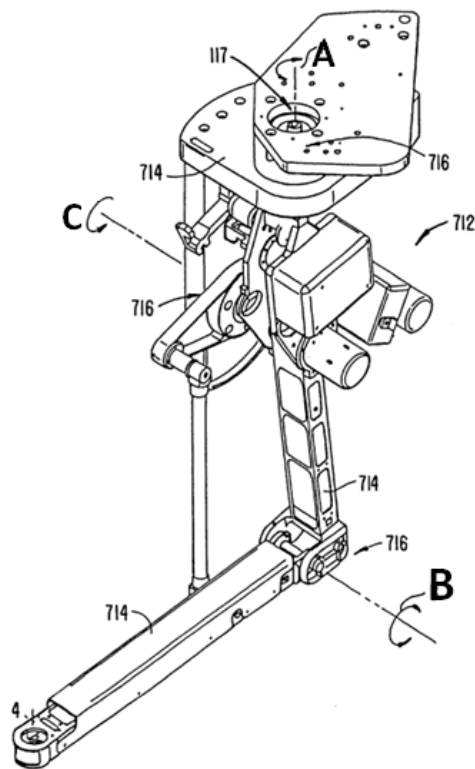
26

Fig. 2-9 The three rotational joints (A, B and C) in the distal part of the master interface.

Mapping between movements of the master interfaces and the slaves manipulators

The controller transforms the spatial motion of the master interfaces into the camera frame of reference, so that the surgeon feels as if his hands are inside the patient's body. The registration, or alignment, of the surgeon's hand movements to the motion of the surgical instrument tips is both visual and spatial. The system projects the image of the surgical site above the surgeon's hands (via mirrored overlay optics), restoring hand-eye coordination and providing a natural correspondence in motions. Furthermore, the controller transforms the spatial motion of the instruments into the frame of reference of the camera, such that the surgeon feels as if his hands are inside the patient's body [27], see Fig. 2-10.
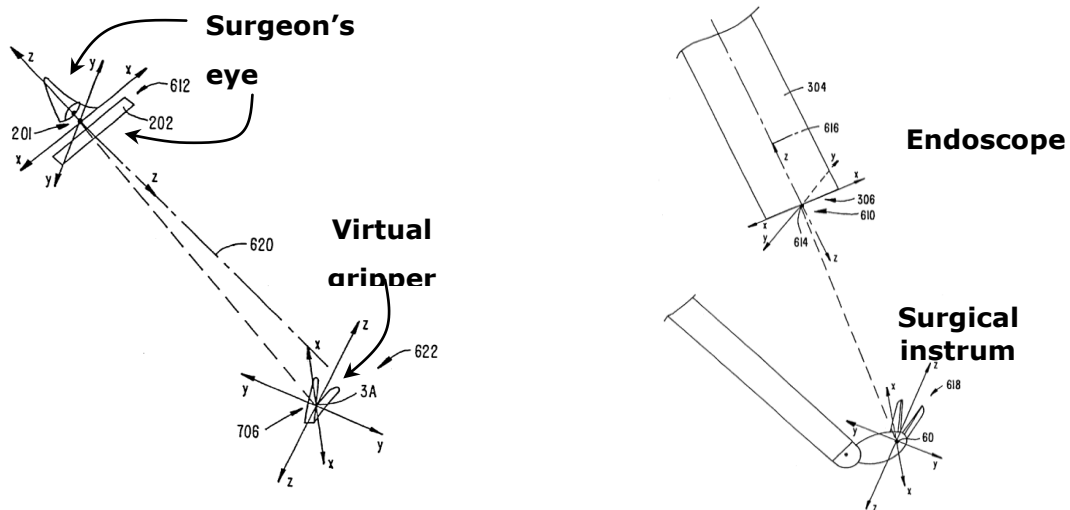
Fig. 2-10 Relation between the eyes of the surgeon in respect to his/her fingers (A) and between the endoscope and the instrument tip (B) (Patent US6364888B1).

The angles between the virtual gripper interface frame, in respect to the display frame, are repeated on the slave, between the end effector frame with respect to the camera frame, by the controller. The end effector frame origin is positioned on the fulcrum of the real surgical gripper, as the virtual gripper interface frame origin is positioned on its fulcrum itself. In this way each rotation around the virtual gripper interface fulcrum is mapped as the same rotation around the real gripper fulcrum.

Relative translation between the virtual gripper interface frame, with respect to the display frame, are repeated by the controller on the slave, between the end effector frame with respect to the camera frame. In this way, if the surgeon using motion scaling 1:1 moves by 1 cm the virtual gripper interface to the left; with respect to the display the surgical instrument gripper fulcrum moves to the left with respect to the camera frame by 1 cm, and so on.

Translations are mapped as relative movements, while rotations are mapped as absolute movements. The use of relative motion control allows a comfortable zero position for the surgeon's arms. The surgeon by pressing his foot on a pedal disengages the master from control of

28

the robotic surgical instruments so that the master can be repositioned for a better alignment [27]. Note that repositioning of master interfaces is possible only on translation DOFs. In fact, if during the repositioning, the surgeon moves also the orientation, the system indicates the need to let go of the virtual grippers but then it restores automatically their orientations to those of the real end-effectors. To do this the master console use motors which are also deployed to reposition the master interfaces to move the slave manipulators whenever needed, e.g., manual repositioning of the manipulators by the assistant, collision between arms or between arms and the patient, etc…). In view of the importance of camera position for optimal viewing, camera movement control is done using the two master interfaces together.

Immersive 3-D viewing

The da Vinci was engineered from its inception to perform telepresence surgery. In this type of surgery, the surgeon is physically and visually separated from the patient, the only contact being the video image. To facilitate telepresence surgery, the computer console purposely isolates the surgeon from his environment. The console hood serves to block the surgeon's peripheral vision. As the surgeon inserts his head into the viewing area and gazes into the binoculars, he descends into the virtual 3D operative field. The surgeon perceives the abdominal or thoracic walls as surrounding him. He is inside the patient [28].

The da Vinci stereoscopic visualization system is comprised of four interconnected subunits. The first unit features a custom-designed endoscope with two separate optic channels with a distance of 6 mm between their longitudinal axis; thus creating stereopsis, which is based on binocular retinal disparity. This is connected to a camera head, which holds two three charge-coupled device (CCD) chip cameras. The image is then processed through a noise reduction system, enhanced, scanned, and then displayed through the stereo viewer, which consists

of two high-resolution monitors, where the surgeon receives a fused 3D image of the operative field [29]. The sterilizable camera is mounted on a slave manipulator and it can be easily moved by the surgeon from the console.

<u>Advantages offered by the robot</u>

Despite its documented advantages over traditional open surgery which benefit both the patient and the hospital health care system, minimally invasive laparoscopic and thoracoscopic surgery imposes major ergonomic restrictions on the operating surgeon which have been highlighted in this review and which increase the level of difficulty in the execution of major abdominal and thoracic operations. Additionally, the manual laparoscopic approach induces surgeon discomfort due to awkward stance and fatigue during long operations. Robot-assisted laparoscopic technology was developed as a solution to overcome these limitations and many researchers have evaluated the effectiveness of the robotic surgical system with respect to manual laparoscopic surgery. These studies have shown that surgical robots can significantly enhance the surgeon's dexterity as well as provide an ergonomically efficient and user-friendly working environment [30].

The most widely reported advantages of the Da Vinci robotic surgery stem from the wristed instrument motions with seven DOF, scaling for precise movements, elimination of hand tremor, and three-dimensional (3D) vision. Magnification and better ergonomics are other advantages that robotic surgery affords over manual laparoscopic surgery. As the tactile and force feedbacks are lost by the laparoscopic approach, the video image provides the only and hence crucial interface between the surgeon and the operative field. In manual laparoscopy, the surgeon operates from a 2D screen while the robotic system allows a 3D natural view integrated within the console [31]. An image in 3D contains more depth cues enabling more accurate and efficient endoscopic manipulations. As monocular depth cues compensate somewhat for the

lack of depth perception in 2D viewing and can provide comparable performance to 3D viewing for some tasks (e.g., distance estimation [32]), it is not surprising that the published literature shows contradictory results on the benefits of the 3D over 2D vision: some studies showing better motor performances with 3D vision while others reporting no differences between the two imaging modalities. This controversy can be partially explained by the fact than all these reported comparative studies, used first-generation 3D systems, with their lower resolution, and eye shuttering technologies (LCD or polarizing glasses) not used in the Da Vinci system which provides immersive stereoscopic vision with true retinal disparity [33]. Some studies have reported that only the complex tasks are performed more easily and more quickly with 3D viewing and demonstrated no difference between two imaging modalities for simple tasks [34]. Other report that the results showed faster performance in 3D than in 2D view for novice subjects while the performance with 2D and 3D was similar in the expert group [31].

In general, the da Vinci system can improve operative performance, especially for inexpert surgeons[35-38].

Most institutions employing robotic surgery systems have based assessment of progress in training and skill level only on subjective evaluations by few experts. This is a serious problem which may be counterproductive to the further growth and dissemination of robotic assisted surgery. To address this problem, recent research has attempted to identify objective variables that can distinguish between skilled and unskilled performance, as well as defining the proficiency-gain curve which confirms the acquisition of the necessary level of skill for safe robotic assisted laparoscopic surgery [38-41]. The use of robotic assistance decreases the learning curve for both standardized tasks and actual operations. However, outcomes data to support these conclusions are scant and much of the data citing the benefits of robotic surgery are based on anecdotal clinical evidence or data from

experiments in dry lab research which are presumed to translate to the situation in the clinical operating room. The da Vinci system would then be used to mentor trainees to a predetermined level of competence and also as a quality-control tool for continued skills assessment [42-43].

<u>Limits of the robot</u>

System malfunctions and robustness

These are well documented in the literature in particular for failures during urologic interventions. A recent survey by Kaushik is based on the retrospective experience of 176 surgeons. One hundred (56.8%) of the 176 responding surgeons had experienced an irrecoverable intraoperative malfunction. Eighty respondents reported mechanical failure before starting RARP (Robotic Assisted Radical Prostatectomy), of which 46 interventions (57.5%) were rescheduled, 15 (18.8%) were performed by an open radical approach, 12 (15%) by standard laparoscopic prostatectomy, and 4 (4.9%) were completed by docking another robot. Sixty-three respondents experienced mechanical failure before starting urethrovesical anastomosis, of which 26 (41.2%) were converted to an open procedure, and 20 (31.7%) to standard laparoscopy; 10 (15.8%) were completed with one less arm, and 3 (4.7%) operations were aborted. Thirty-two respondents experienced malfunction before completion of the anastomosis, of which 20 (62.5%) were converted to standard laparoscopy, and 12 (37.5%) were converted to open surgery. This retrospective study gives no details on the nature of the component malfunction and, furthermore it is entirely based on retrospective experience of the surgeons rather that on actual number of cases and thus give no indication of the failure rate of the Da Vinci robot for this specialty.

Nayyar [44] reported a percentage critical mechanical failures that determined conversion rate of 0.6% in a retrospective study of 340 cases (2 critical malfunction) in a total of 37 incidents during surgery (10.9%). This author emphasizes the importance of a complete

preliminary check to ensure proper functioning of every component of the robot before induction of anesthesia since many malfunctions can be recognized before surgery commences. Borden [45] reports a similar percentage failure rate. Nine of the 350 (2.6%) scheduled RLRPs could not be completed robotically because of device malfunction. Six of the malfunctions were detected prior to induction of anesthesia when surgery was rescheduled. The etiology of the malfunctions included: set-up joint malfunction (2), arm malfunction (2), power error (1), monocular monitor loss (1), camera malfunction (1), metal fatigue/ break of surgeon's console hand piece (1) and software incompatibility (1). Three malfunctions occurred intraoperatively (0.86%) and were converted either to a conventional laparoscopic (1 case) or an open surgical approach (2 cases). No details of the nature of the robot failures are provided in this report.

Two similar studies, with larger case series, report lower percentage critical malfunction rate during the intervention. Lavarey in 2008 reported the results of a questionnaire regarding the number of equipment malfunctions during RALP, the number of procedures that had to be converted or aborted, and the component of the robotic system that malfunctioned. Eleven institutions participated in the study with a median surgeon volume of 700 cases, accounting for a total case volume of 8240. Critical failure occurred in 34 cases (0.4%) leading to the cancellation of 24 cases prior to the procedure, and the conversion to two laparoscopic and eight open procedures, with a total of 10 critical malfunctions that determined conversion (0.12%). The most common components of the robot to malfunction were the arms and optical system [46] but it is not clear which component malfunctions determined the conversions.

In a single institution study by Kim in 2009 [47], insurmountable malfunction during interventions in general surgery, obstetrics and gynecology, thoracic surgery, cardiac surgery and otorhinolaryngology, mechanical failure or malfunction occurred during robotic surgery in 43

cases of 1797 (2.4%). This report does not provide clear details on the number of malfunctions that determined the cancellation of the intervention. It simply reports that malfunctions determined conversion in 3 cases (0.17%). One open conversion was performed due to a malfunction of the console arm in radical prostatectomy. Two laparoscopic conversions were performed, one due to wire cutting of the console arm during radical prostatectomy and once because of a malfunction of the robotic arm during gastrectomy. However these malfunctions are not clearly described and may have been the result of human error rather than machine failure.

Many recoverable mechanical problems during surgery are related to the robotic instruments due to various types of malfunction, including broken tension wires or wire dislodged from the working pulleys (since wire transmission used for EndoWrist instruments is weak), non-recognition of the instrument by the robot (despite available residual use) and locked instrument. However these types of errors can be corrected or bypassed albeit with some additional operating room time.

The low rate of technical problems is probably the consequence of the system characteristics: big and robust mechanical mechanisms and the use of traditional and established technology   for building links, joint and power transmission (excepting those of the surgical instruments). Several studies have concluded that operative time is generally prolonged by the use of robotic surgery systems. Some studies directly incriminate the robotic set-up as a significant source of extra time. Iranmanesh et al disagree with this conclusion as both draping and docking of the da Vinci surgical system have a steep learning curve and neither of them, when performed by designated and well-trained teams, incur a significantly negative influence on overall OR times[48].

Lack of tactile feedback

The da Vinci surgical telemanipulator does not offer any kind of haptic feedback. This is a major disadvantage particularly during the execution of complex tasks [40]. The two important adverse consequences of this loss of tactile feedback during laparoscopic robotic surgery are the inability for the surgeon to identify tissue consistency enabling discrimination between tumor and normal tissue[49], and the execution of intracorporeal suturing and knot tying especially with fine suture material [50-52].

Robot workspace and the importance of an optimal port placement

The ability to determine the optimal position of the robot and the location of the incisions has a significant impact on the surgeon's ability to perform expeditiously the surgical procedure. Hence, surgical planning is a critical aspect of efficient minimally invasive robotic surgery. Thus optimal port location [4] is essential for maximizing the performance of the robot. Apart from robot dexterity and the ability to reach the entire surgical field, there are other factors that must be considered when selecting port locations. In general port positioning has to avoid collision between the arms of the robot (external to the patient), other obstacles in the operating room and the patient. Other considerations include collision avoidance between the surgical instruments (inside the patient's body); interference avoidance between the tools and the camera field of view; and preservation of the surgeon's intuition by maintaining the relative orientation between the surgeon's hands and eyes. One study [53] revealed that with a larger workspace the ports can maintain an adequate distance between the robot arms to avoid external collision, especially when both arms are actively working, whereas in a smaller workspace the distance between the ports becomes reduced and thus prevents optimal functioning.

The workspace reachable by a single robot arm is large (as many of the rotational joint can be rotate through 360°) and intra-arm collisions are

limited because of the arms design. However, the workspace can be limited with simultaneous use of two (or three) arms due to collision. In addition to the possible collision between instruments shafts (as with manual laparoscopic surgery), there is the risk of possible inter-arm collision between the external parts. In particular, rotation of the entire remote centre of motion mechanism (supporting the instrument rail) can determine many collisions. With closely positioned access ports (4-5 cm) when the target field is deep, the external parts of the arms can come to lie almost parallel with an increased risk of collision.

Future developments

Ongoing research is addressing existing deficiencies of robotic surgery, e.g., haptic feedback[54], enhancement of the system integration, and augmented reality navigation system[55]. Other research is aimed at resolving outstanding training issues including the next generation of virtual reality simulators[56]-[57]. Miniaturization of components and systems will be required if surgical robots are to reach their full potential. Work in this direction is progressing and the feasibility of an intracorporeal robotic device has been demonstrated. Much further work is required to refine current design concepts for clinical application[58]. To date, researchers in this field have demonstrated that small fully implantable robots can be manipulated from the outside with much less force and trauma to the tissues, allowing for more precision and delicate handling of tissues. The evolution of miniature robots is, however, still in a developmental stage and is being tested in animal models [59-60]. The next step would be to refine these technologies further to empower the surgeon with augmented real-time visualization of tissue and intracorporeal dexterity, possibly even through a single port.

This review has highlighted advantages and motivations of few drawbacks of daVinci surgical system. Then Medical robotics has great potential to revolutionize clinical practice not only for minimally invasive surgery but for overall oncologic workflow: planning, diagnosis,

treatment, surgery and training. In this context it is integrated a robot in a generic CAS platform (chapter 3) and a potential application has been implemented (chapter 5).

3 Integration of a Robot in a image guided system

3.1 Introduction

This chapter describes how to integrate a robotic arm in an image guided system in order to control end effector position in respect to a global reference frame used to plan and to guide the intervention.

Studies and tests were performed using a 6 DoF (Degree of freedom) industrial robot Samsung FARA AT2 (Fig. 3-1). As previously written, the robot has been integrated in the EndoCAS Navigator platform.

The robot is equipped with a low level controller that implements the position control, managing the direct and inverse kinematic of the robot. It was developed a C++ software module to manage the communication with the robot controller. The communication between the low level controller and the Personal Computer is performed via Ethernet. It is possible to command to the robot to move its end effector to a specific position and orientation in terms of Cartesian space, referenced to the robot reference system, or in terms of joint space, imposing specific angles for each joint.

Fig. 3-1 The robot Samsung

The robot has been sensorized with an optical sensor to be tracked by the optical Localizer(NDI Optotrak). The sensor is positioned for three reasons. At first to track medical instruments managed by the robot,

the second to obtain a closed loop control and the third one to refer robot position respect to the global frame.

To move the robot end effector in respect to the global reference system, generally fixed or linked with the localizer, it is necessary to determine the geometric relation between the robot end-effector (E reference system) with the sensor frame (F reference system) and between the global reference system (O reference system) and the robot reference system (R reference system).
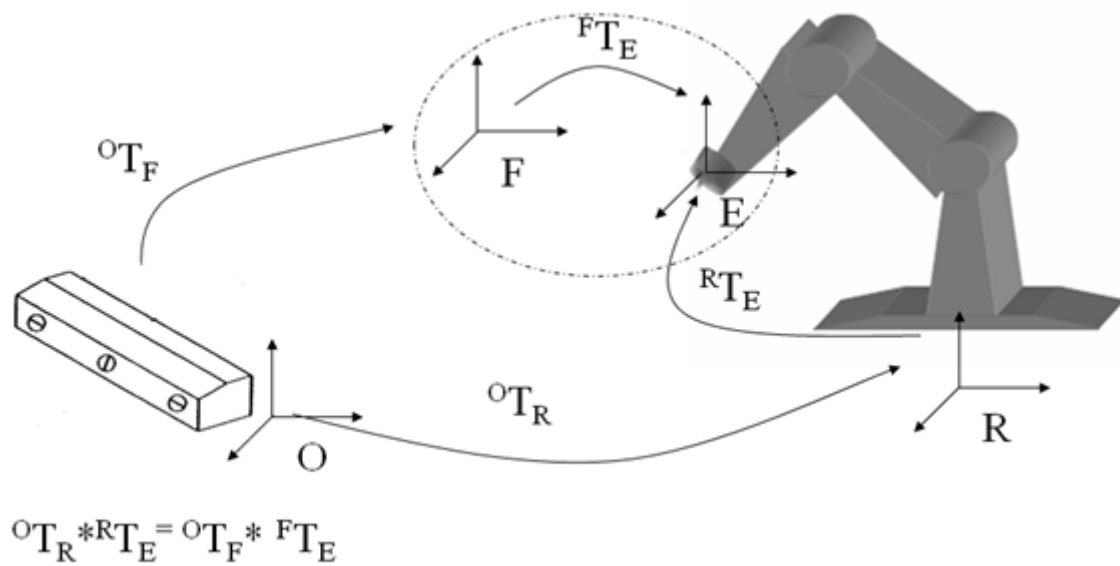

Fig. 3-2 Reference systems involved in the robot-localizer calibration, are :R= Robot Frame ; O= Global Frame; E= End-Effector Frame; F= optical sensors Frame.

The transformation chain describing the relation between the four reference frames is:

$$^{O}T_R*^{R}T_E=^{O}T_F*^{F}T_E \qquad (1$$

Where the transformation $^{O}T_F$ from the Optotrak base frame to the sensor frame (Fig. 3-2) is known by means of the lecture of the position sensor; $^{R}T_E$ is the transformation between the robot base frame to the end-effector frame, which is determined by the robot controller, which read joint encoders and calculate direct kinematic; $^{O}T_R$ is the transformation from the Optotrak base frame to the Robot base frame,

which is unknown; also the transformation ^FT_E, from the end-effector frame to the sensor frame is unknown. The problem can be summarized in the simultaneous calculation of the last two unknown spatial relations.

Knowing ^OT_R and ^FT_E it is possible to completely describe the transformation chain and so to control the robot end effector in the global reference frame (O), to track in real time robot end effector (and so a surgical instrument fixed on it), to control in a closed loop end effector right positioning.

The solution adopted in this thesis to calculate ^FT_E and then ^OT_R is shown in the following paragraph.

3.2 Robot Calibration

This problem is the same, in terms of transformation to determine, as another calibration problem, extremely important in the field of robotics, known as the "hand-eye" calibration problem, where a camera ("eye") is mounted on the end effector ("hand") of a robot. For us the sensor can be considered as the camera in the "hand-eye" calibration problem. A number of different solutions have been developed for this problem. The classical approach is "Move the hand and observe/perceive the movement of the eye". The major part of existing solutions brings back to the resolution of a equations system of the type:

$$A \times X = X \times B \qquad\qquad (2$$

where A, B and X are transformation matrices.

It is possible reports the calibration process of the robot-localizer to the resolution of above equation, considering the reference frames in two robot poses, as shown in the following figure.
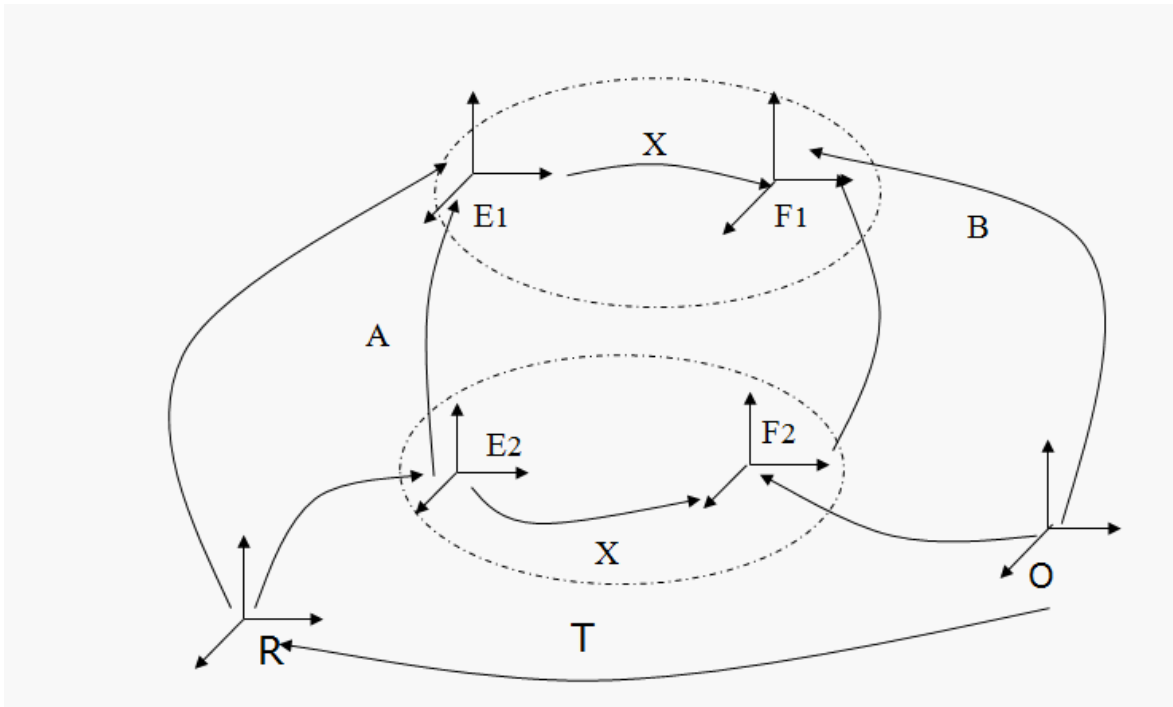
Fig. 3-3 Schematic representation of the AX=XB problem ; A: matrix describing the position and orientation of the sensor frame relative to itself after the movement arbitrary; B: matrix that describes the position and orientation of the end effector with respect to himself after the same movement; X: matrix that describe the static relation between the end effector and the sensor frame, ($^{E}T_{F}$)

To obtain an unique and exact solution it is sufficient only two pair of (A_i,B_i) satisfying some condition (independent movements).

But there are measure errors due the sensors. In particular, industrial robots are designed to be highly repeatable, but not very precise. For the Samsung robot the accuracy measured is of several millimeters (it was experimentally measured an worst case error of 7mm). Therefore K measures are performed to determine K couples (A_i, B_i). Given a set of N measurements of A and B, find X such that satisfies

$$A_1 \times X = X \times B_1$$

$$\vdots \qquad \vdots$$

$$A_2 \times X = X \times B_2$$

$$\vdots \qquad \vdots$$

$$A_N \times X = X \times B_N$$

Most approaches decompose the matrix X into its rotational and translational part and optimize for first the rotation and then the translation. The first works were of Shiu and Ahmad[61] (least squares fitting of rotation, then translation, using angle-axis representation) and Tsai and Lenz [62] (similar to [61] with closed form solution). Zhuang and Roth [63] simplified the formulation introducing quaternions for the estimation of the rotational part, in the same way as Chou and Kamel [64], who make use of the singular value decomposition (SVD). Park and Martin [65] perform nonlinear optimization using Euclidean Group. Zhuang and Shiu [66] apply nonlinear optimization for both parts, Fassi and Legnani [67] give a geometrical interpretation of these equations, making use of rototranslation and screws. Daniilidis [68] introduces the dual quaternions, an algebraic representation of the screw theory to describe motions. This enables the author to find a fast SVD-based joint solution for rotation and translation within linear formulation. Dornaika and Horaud [69] solve the rotational problem linearly with quaternions and also nonlinearly optimize both parts by one-to-one minimizing of Frobenius norms and two penalty functions.

For this work, it was used an approach which was developed by Park and Martin in [65]. Despite the theoretically complexity of the algorithm (it is based on the matrix logarithm of the transformation matrix) it is extremely easy to implement.

Let $\Theta \in SO(3)$ be any rotation matrix and let be $b \in \mathbb{R}^3$ be the translation. Therefore, any valid transformation matrix M has the form:

$$M = \begin{bmatrix} \Theta & b \\ 0 & 1 \end{bmatrix}$$ (3

If $trace(\Theta) \neq -1$, the logarithm of this matrix is

$$\log M = \begin{bmatrix} [\omega] & A^{-1}b \\ 0 & 0 \end{bmatrix}$$ (4

where

$[\omega] = log\Theta$ and A is a matrix whose is irrelevant for solving the calibration problem.

Let be

$$\phi = cos^{-1}\left(\frac{trace[\theta]-1}{2}\right) \tag{5}$$

The matrix logarithm $[\omega]$ is

$$[\omega] = \frac{\phi}{2\,sin\,\phi}(\Theta - \Theta^T) \tag{6}$$

This is a skew symmetric matrix

$$[\omega] = \begin{array}{ccc} 0 & -\omega_3 & \omega_2 \\ \omega_3 & 0 & -\omega_1 \\ -\omega_2 & \omega_1 & 0 \end{array} \tag{7}$$

Therefore, $[\omega]$ can be parameterized as the vector $[\mu]$ where

$$[\mu] = \begin{bmatrix} \omega_1 \\ \omega_2 \\ \omega_3 \end{bmatrix} \tag{8}$$

The Park-Martin algorithm [65] attempts to find X

$$X = \begin{bmatrix} \Theta_x & b_x \\ 0 & 1 \end{bmatrix} \tag{9}$$

Equations that satisfied the hand-eye equation , and then the X is determined minimizing:

$$e = \sum_{i=1}^{k} d(A_i X, X B_i)$$

where d(.. .) is some distance metric on the Euclidean group.

Using the canonical coordinates for Lie groups the above minimization problem can be recast into a least-squares fitting problem that admits a simple and explicit solution. Specifically, given vectors $x_1, x_2, x_3, \ldots x_k$ and $y_1, y_2, \ldots, y_k$ in Euclidean n-space it was provided explicit expressions for the orthogonal matrix Θ and translation b that minimize

$$\eta = \Sigma_{i=1}^{p}\|\boldsymbol{\Theta x_i} + b - y_i\|^2$$

The best values of Θ and b turn out to depend only on the matrix

$$M = \sum x_i y_i^T$$

By applying the canonical coordinates and this result a "best-fit" solution to AX = XB can be obtained. The AX=XB can be expressed in term of rotational and translation part:

$$\begin{pmatrix} \Theta_A & b_A \\ 0 & 1 \end{pmatrix} \begin{pmatrix} \Theta_x & b_x \\ 0 & 1 \end{pmatrix} = \begin{pmatrix} \Theta_x & b_x \\ 0 & 1 \end{pmatrix} \begin{pmatrix} \Theta_B & b_B \\ 0 & 1 \end{pmatrix}$$

The algorithm decomposes the solution into two sub problems. The first is to calculate the rotation of Θ_x, which can be carried out independently of the translations. The second problem calculates b_X using the calculated value of Θ_x.

$$\boldsymbol{\Theta_A \Theta_X} = \boldsymbol{\Theta_X \Theta_B} \qquad\qquad (10$$

$$\boldsymbol{\theta_A b_X} + \boldsymbol{b_A} = \boldsymbol{\theta_X b_B} + \boldsymbol{b_X} \qquad\qquad (11$$

$$(\boldsymbol{\Theta_A} - I)\boldsymbol{b_X} = \boldsymbol{\Theta_X b_B} - \boldsymbol{b_A} \qquad\qquad (12$$

The rotation matrix Θ_x is chosen to minimise the cost function:

$$\boldsymbol{\eta_1} = \Sigma_{i=1}^{p}\|\boldsymbol{\Theta_X} \cdot \boldsymbol{\beta_i} - \boldsymbol{\alpha_i}\|^2 \qquad\qquad (13$$

Let α_i be the matrix logarithm of measurement a_i and β_i be the matrix logarithm of measurement B_i.

The optimal solution is

$$\boldsymbol{\Theta_X} = (\boldsymbol{M^T} \cdot \boldsymbol{M})^{-1/2} \cdot \boldsymbol{M^T} \qquad\qquad (14$$

where

44

$$M = \sum_{i=1}^{p} \beta_i \cdot \alpha_i^T \tag{15}$$

If the number of measures $p = 2$, the third measurements are synthesized as $\alpha_3 = \alpha_1 \times \alpha_2$ and $\beta_3 = \beta_1 \times \beta_2$. The matrix M has the property that it is always guaranteed to be orthonormal even if the data is noisy. The second optimization solution minimizes

$$\eta_2 = \sum_{i=1}^{p} \left\| (\boldsymbol{\Theta}_{A_i} - I) \cdot b_X - \boldsymbol{\Theta}_X \cdot b_{B_i} + b_{A_i} \right\|^2 \tag{16}$$

This can be expressed as a standard least squares minimization problem and its solution is

$$b_X = (C^T \cdot C)^{-1} \cdot C^T d \tag{17}$$

Where

$$C = \begin{bmatrix} I - \boldsymbol{\Theta}_{A_1} \\ \vdots \\ I - \boldsymbol{\Theta}_{A_p} \end{bmatrix} \tag{18}$$

and

$$d = \begin{bmatrix} b_{A_1} - \boldsymbol{\Theta}_X \cdot b_{B_1} \\ \vdots \\ b_p - \boldsymbol{\Theta}_X \cdot b_{B_p} \end{bmatrix} \tag{19}$$

This equation can be solved even if only two measurements are used. A problem that is common to all hand-eye calibration algorithms is that the quality of the result is highly dependent on the data used for computing the unknown transformation. The usual approach for solving this problem is to use robot movements that already take the restrictions on the data into account, which means that the movements has to be planned before recording.

It has been developed a routine in Matlab and imported in a Visual C++ application. The determination of the unknown matrix is totally automatic. Starting by a initial position the robot moves inside a fixed workspace (translation part [-100, 100], orientation part [-10, 10]) a random component in the movement was added, ensuring to remain in the workspace and to cope the entire workspace. The robot is stopped

in each new position to avoid measurement noise due to mechanical vibrations. The routine acquires position and orientation of the robot end-effector (E) and position and orientation of the optical sensors frame (F). At the end of all movements is calculated as described the transformation matrix X, from the end-effector frame to the sensor frame, corresponding to $(^{F}T_{E})^{-1}$, described in the previous paragraph (Fig. 3-2). Then $^{O}T_{R}$ can be calculated inverting equation (1):

$$^{O}T_{R} = {^{O}T_{F}} * {^{F}T_{E}} \, {^{E}T_{R}}$$

In the Visual C++ application they are integrated the optical localizer Optotrak and the electromagnetic localizer Aurora.

After calibration the robot can be integrated in the imaged guided system and it can be moved along planned trajectories and in a closed loop with the global reference system.

4 Integration of ultrasound imaging in an image guided system

Ultrasound imaging is a non invasive method that reveals important diagnostic information from patients. It is more diffused and cheap in respect to other medical imaging modalities such as CT and MRI. 2D ultrasound is easy to use and rapidly provides images from a hand held probe. The operator holds the probe in contact with the patient's body and the ultrasound scanner produces real-time images of the anatomical structure within the cross-sectional plane of the probe. The probe excites pulse of ultrasound energy that propagate through the patient's body; the same probe also receives echoes of the energy from the anatomical structures. In response to these echoes, the probe produces electric signals back to the scanner for the reconstruction of an ultrasound image. The generation of the image is based on the principle that the depth of the various anatomical structures can be computed by multiplying the propagation speed of the pulse and the elapsed time of the echoes. Brightness of the image corresponds to the strength of the echo. This is called the pulse echo principle that is cornerstone of the ultrasound imaging technology.   A drawback of ultrasound imaging is that it doesn't work well under bones or gas because the ultrasound energy is almost completely reflected.

Two-dimensional ultrasound imaging is widely used in clinical practice because is an inexpensive, compact and highly flexible imaging that allows users to manipulate a probe in order to view various anatomic structures. It is use in the phase of diagnosis and as guidance in percutaneous treatments. However the use of 2D Ultrasound imaging present some disadvantages it requires that the users mentally integrate many images to reconstruct an impression of the anatomy in 3D. The probe is controlled free-hand therefore it is difficult to relocate anatomic positions and orientations and repositioning of the probe at a particular location, when scan a patient.
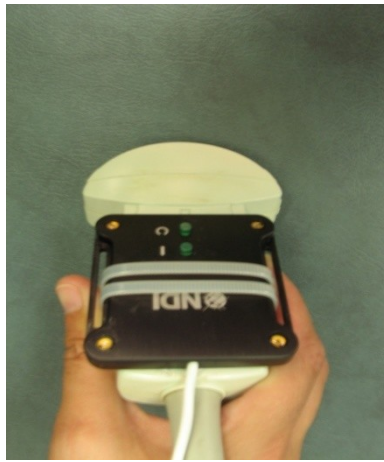
Fig. 4-1 US probe with attached an optical sensor

These limitations can be overcome inserting the US imaging in a image guided system, then providing a mixed reality view where the US scan plane is shown in respect to other information, for example a 3D model of the anatomy and/or surgical instruments (Fig. 4-2).
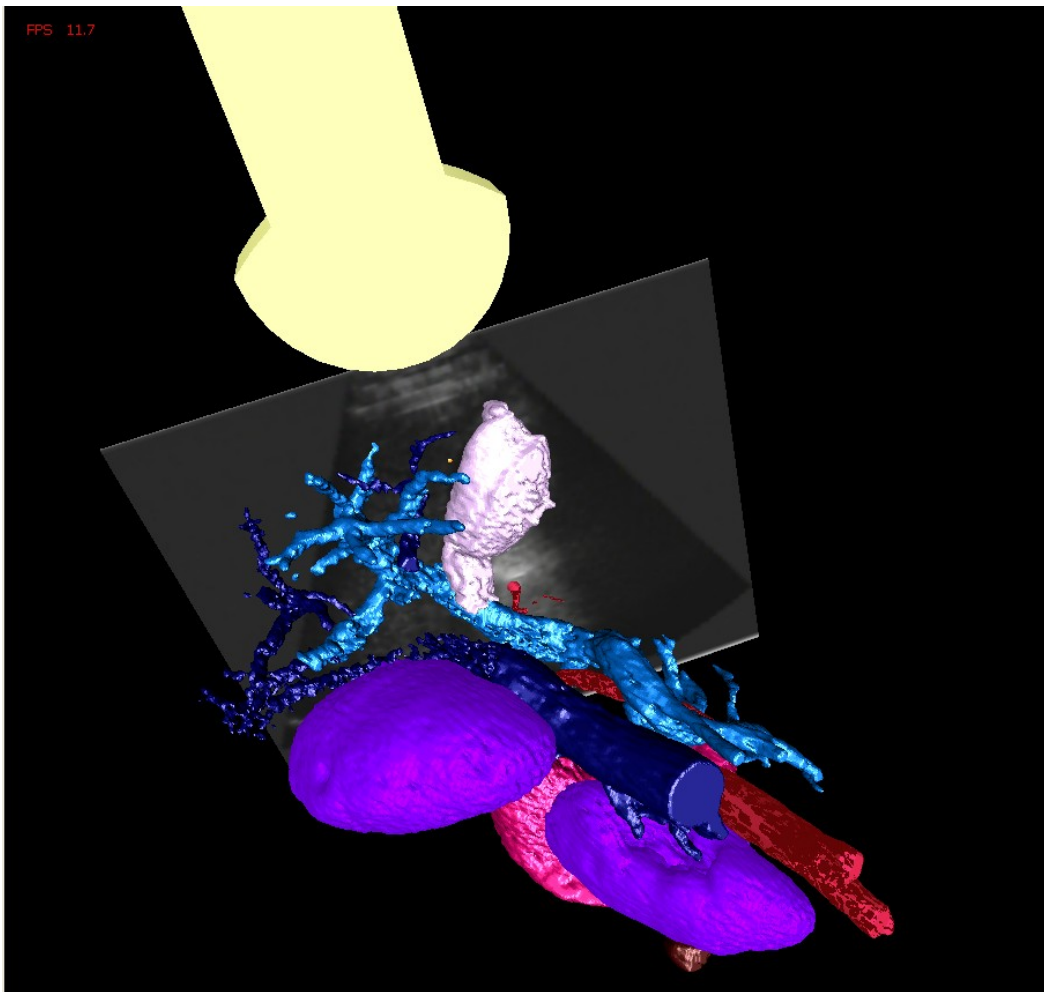

Fig. 4-2 Mixed reality view

To show the US scan plane in the right position can be used an external tracking system to measure the position and the orientation of the probe. The tracking system indirectly measures the positions of the US scan plane by measuring the sensor attached to the probe handle(Fig. 4-1). Calibration routine for sensors positions on the probe handle is required, to determine the transformation between the coordinate systems of the sensor and the US images. Calibration play a critical role in determining the overall accuracy of a tracked 2D ultrasound system.

4.1 Ultrasound Calibration

Several articles have been written concerning the development of calibration techniques for freehand 3-D US system[70-84]. Performing calibration by scanning an object with known geometric properties (phantom) has been a research topic for many years. It involves taking enough images of an object with known dimensions, in which a transformation from the image space to the object space is possible. These scans place constraints on the eight calibration parameters: 2 image scales, 3 translations in the direction of the x, y and z axes and the three rotations—azimuth, elevation and roll—about these axes. Sometimes the scales may be supplied by the manufacturer. The most prevalent set-up to determine these parameters, consists of a tracking device, an ultrasound probe coupled with a tracking sensor, and a phantom. Similar setups involves the following reference frames: the ultrasound image (P), the probe tracking sensor (R), the tracking device T, and the phantom C. The overall transformation chain can be expressed as a single equation of homogeneous transformations that determines the coordinates of a point respect to the plane reference frame in the coordinates respect to the phantom reference frame.

$$C_x = {}^{C}T_T \, {}^{T}T_R \, {}^{R}T_P \begin{pmatrix} s_x u \\ s_y v \\ 0 \\ 1 \end{pmatrix}$$
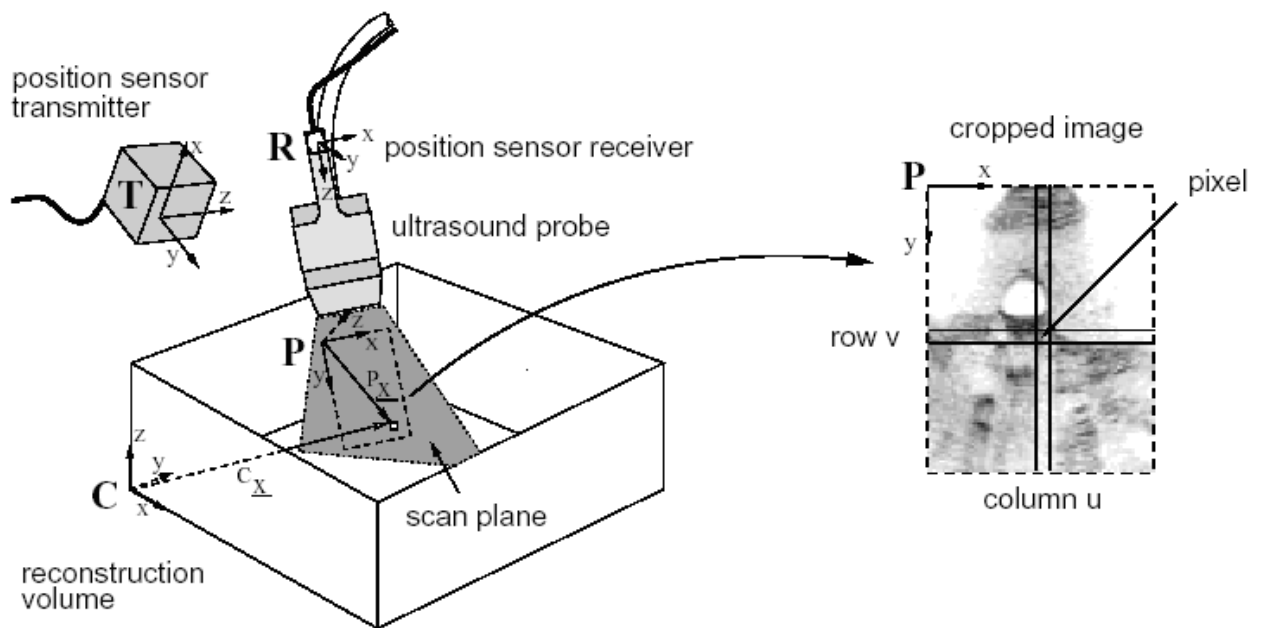
Fig. 4-3 An overview of the calibration process. The ultrasound image frame P, the ultrasound probe frame R, the tracker frame T, and the reconstruction volume frame C are all apparent ([85])

A variety of trade-offs exist in selecting a calibration method. Some of the pertinent factors that need to be considered are the complexity and cost of phantom construction, the length of time required for the calibration data collection and post processing task, the necessary precision and accuracy with which the phantom needs to be constructed for the calibration to work effectively and the degree of difficulty of obtaining quality images of the phantom over the range and orientations that are necessary to make the calibration problem well-conditioned. New methods continue to appear and differ mainly in terms of the geometrical properties of the phantoms to achieve more accurate calibration results o easier processing step than previous methods. The majority of the methods can be classified according to four kinds of phantoms: wire, plane, precalibrated tracking pointer and irregularly shaped phantoms. Much of the research pertaining to 3-D US calibration has focused exclusively on the development of calibration techniques that drastically reduce the number of images that need to be collected to attain a successful calibration ([84]). Unfortunately, a decrease in the number of images necessary to complete a calibration necessitates

an increase in the complexity and difficulty of calibration phantom construction and/or the necessary precision with which the calibration phantom must be constructed for the phantom to be functional. There are a number of different calibration methods reported in the literature.

<u>Single Point Targets</u>

The phantom can be as simple as a point target. Indeed, this was one of the first phantoms ([76, 86]) used for this purpose and it was used for many time ([87-88]). State et al. [86] scanned a 4mm bead suspended at the tip of a pin. Detmer et al. [76] used cross-wire phantoms and scanned the intersection of the wires, which appear as a single point. The idea in both cases is to image a point and to locate this point in the B- scan as well as the world space. Segmentation of this point on the B-scan is usually performed manually, although some automatic techniques exist, but they are not reliable due to the poor ultrasonic image quality. If the coordinates of the volume are aligned to have its origin at this point, for a cross-wired phantom, then the pixel at the crossing should satisfy

$$
\begin{pmatrix} 0 \\ 0 \\ 0 \\ 1 \end{pmatrix} = {}^{C}T_{T} \, {}^{T}T_{R} \, {}^{R}T_{P} \begin{pmatrix} s_{x}u \\ s_{y}v \\ 0 \\ 1 \end{pmatrix}
$$

The first three rows give rise to three active constraints that need to be satisfied. If n scans of the point are performed from different directions and orientation, it is obtained a set of 3n constraints. The solution can be solved using iterative optimization techniques, such as the Levenberg-Marquardt algorithm [89].

Muratore and Galloway [83] and Peria et al [90] scanned the tip of a moving tracked pointer while keeping the probe stationary. The tip of the pointer was placed at various positions of the B-scan. These points were manually segmented in the ultrasound images. This sets up the same system of equations, with the spatial locations of each point

obtained from the tracked pointer. The mapping from the tracked pointer centre to its tip was supplied by the manufacturer, and so it does not require any calibration to determine this transformation.

Three Wire Phantom

Another wire phantom is the three wire phantom. Instead of mounting a pair of cross-wires in the solution, three mutually orthogonal wires are mounted. These three wires form the three principal axes of the phantom coordinate system as shown in Fig. 4-4. Each wire is sequentially scanned along its length. The wires appear as a dot on the B-scan.
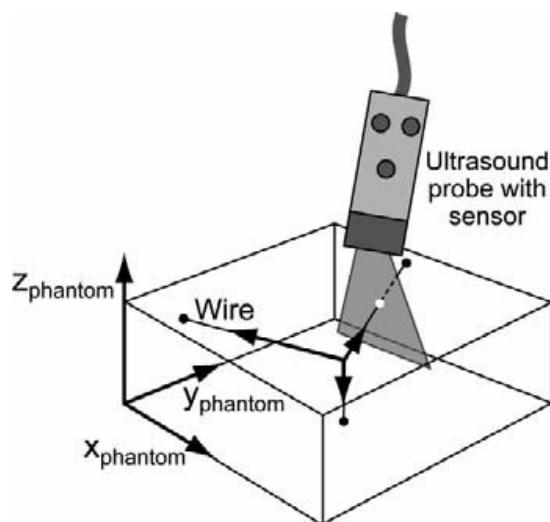

Fig. 4-4 Three wire phantom

This method is better than the previous point target in the sense that it is easier to scan along a line rather than trying to maintain a point target in the middle of the thick ultrasound beam. It is necessary to keep track which of the three axes are scanned at any one time. The accuracy of this system depends on the orthogonality and straightness of the three wires. The difficulty in segmentation of the wire is that the wire does not appear as a point or a circular dot. The image is corrupted by the acoustic nature of ultrasound images. Semi-automatic segmentation of the point has being implemented by Carr et al. [15]. The user defines a region where the wire appears on the image and an

automatic algorithm searches for the centroid of the wire. This allows more accurate and faster segmentation.

Wall phantoms.

Instead of scanning a point, it is possible to scan a plane. The design complexity of the plane varies from the floor of a container ([85, 91], a plexiglass plate [91], a nylon membrane [92-93] to a precision-made Cambridge phantom [85] and its variants [94-95]. All wall methods proposed produce a line on the US image, which is attractive because image information for the line is more redundant, making it easier to segment than points. If a line is partially missing, it can still be easily estimated, which is not the case for points. The simplest wall method, the single-wall technique [85] is based on imaging the floor of a water tank. One problem with this method is that specular reflection causes low returning intensity at oblique scan angles. Furthermore, it is difficult to determine the true position of the floor in the images, solely based on reflected signal intensity. This is due to the strong reverberations from the bottom, which appear like a "comet tail" in the reflected intensity signal. The membrane technique solves the reverberation problems of the first, by imaging a thin membrane instead of the bottom of the tank. Hence, this solution produces thinner lines on the images. Care must be taken, however, to choose a membrane rigid enough to minimize the membrane oscillation caused by the movements of the probe in water [93]. In both cases, difficulties arise when imaging at an angle far from the normal. In the first case, most beams will be reflected away from the probe because of specular reflection, yielding a lower intensity line. In the second case, the line on the image will lose its sharpness, because of the US beam thickness. In the case of the single-wall phantom, simply roughening the bottom of the tank helps to compensate for the specular reflection problem. Mathematically, the plane is considered to be at $z = 0$, with the z-axis orthogonal to the plane; hence, the two phantoms above are described by:

$$\begin{pmatrix} x \\ y \\ 0 \\ 1 \end{pmatrix} = {}^{C}T_T {}^{T}T_R {}^{R}T_P \begin{pmatrix} s_x u \\ s_y v \\ 0 \\ 1 \end{pmatrix}$$

The Cambridge phantom [85] was created to solve the problems mentioned above. The probe is attached in a clamp in such a way that the top of a thin brass bar is always in the center of the beam (Fig. 4-5). To ensure this alignment, Prager et al describe a separate technique including another piece of equipment.
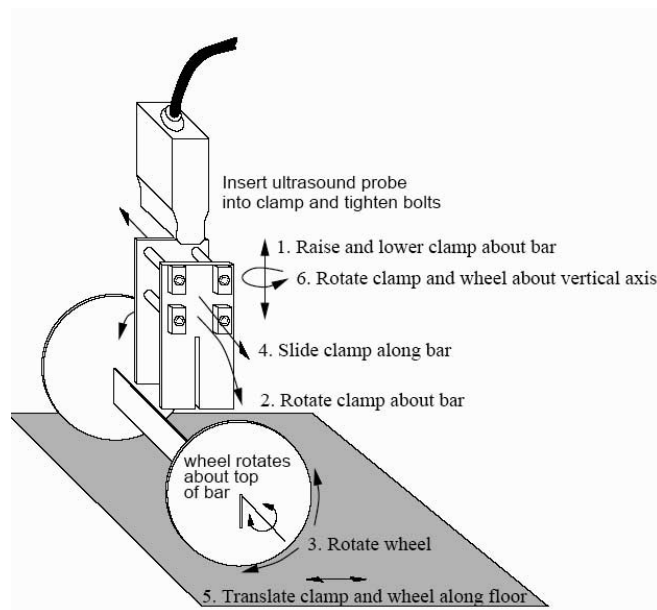

Insert ultrasound probe
into clamp and tighten bolts

1. Raise and lower clamp about bar

6. Rotate clamp and wheel about vertical axis

4. Slide clamp along bar

2. Rotate clamp about bar

wheel rotates
about top
of bar

3. Rotate wheel

5. Translate clamp and wheel along floor

Fig. 4-5 Cambridge Phantom

After alignment, the phantom is immersed in a water bath; the clamp with the probe is placed over the bar and the bar is scanned from all possible angles, subject to the constraints imposed by the setup. The top edge of the bar acts as a virtual plane, yielding a line in the US image that is sharper and of relatively higher intensity. The wall methods are among the quickest solutions for calibration, due to the possibility of automatic extraction of the lines in the US images.

<u>Two-Dimensional Alignment Phantoms</u>

When calibration is performed using a point phantom with the aid of a stylus, with known scales, calibration only needs three non-collinear points to be positioned in the scan plane. If it is possible to align the scan plane with three such points at the same time, then even one frame is sufficient for calibration. Sato et al [96] were the first to use such a phantom. They scanned a thin board with three vertices as shown in Fig. 4-6.
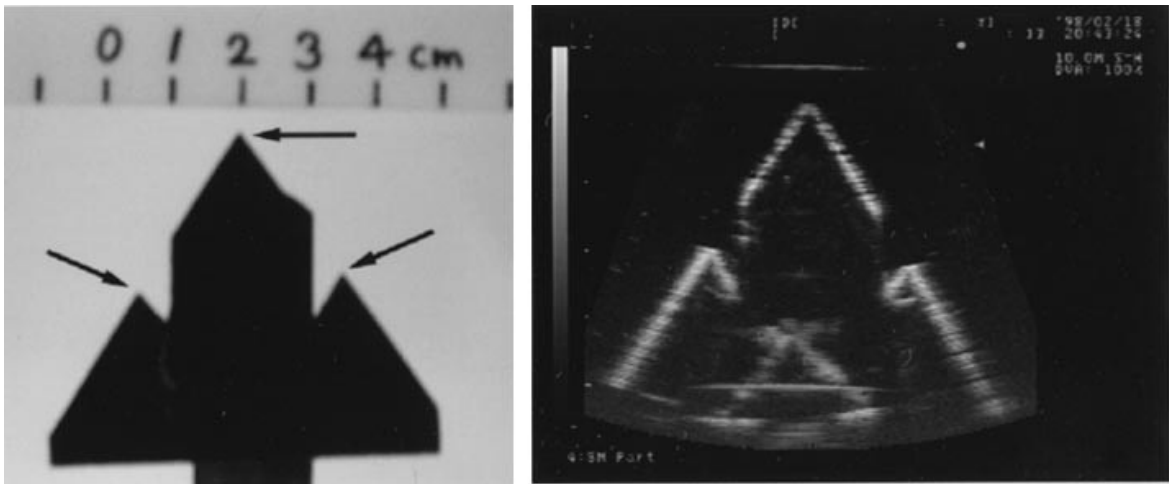

Fig. 4-6 2D alignment phantom

The main difference between two-dimensional phantoms and those classified as point phantoms is that the position and orientation of the two-dimensional phantom are fixed and hence known in space using specific devices. Therefore a single scan locating three points in the plane is sufficient for constraining the six degrees of freedom between the probe and the receiver. Contrary for a point target, there is an additional three parameters between the target and the reconstruction volume. The governing equation for this type of phantom is to transform the points located in the B-scan to the transmitter's space by:

$$x_T = {}^T T_R \, {}^R T_P \, x_P$$

There are in general two ways of determining the phantom's 3D location in the transmitter's space. The first is to locate fixed points on the phantom using a 3D localizer (pointer). A pointer was used by many

researchers [81, 90, 96-98], and their colleagues to locate the phantom in world space. The pointer measurement is of course subject to experimental errors, albeit small. Welch et al. [98] averaged 100 measurements of localized points on the phantom. The other common approach is to attach fixed markers on the phantom itself so that they can be detected by the transmitter. The phantom features to be scanned need to be accurately manufactured in known positions relative to the attached markers. One advantage of using this approach is that the phantom may be moved with its attached markers during calibration. This approach was adopted by Bouchet et al. [73] and [82]. Comeau [74], Pagoulatos [84] and their colleagues used a combination of the two approaches. The phantom was designed with all features relative to a divot on the phantom itself. The position of this divot is then obtained by using a pointer. Peria et al. scanned a triangle formed by wires in a water tank and then manually segmented the vertices in each B-scan. The location of each vertex in the transmitter's coordinate system is located by using a 3D pointer. The ultrasound image scales can be estimated from the segmented vertices, since the dimension of the phantom is known. Three distinct points are thus located in both the transmitter (hence receiver) and the ultrasound probe's coordinate systems. The transformation between the two coordinate systems could then be solved. Due to the small number of points located, a closed form solutions is feasible. The main disadvantage of using a two-dimensional phantom is that it is very difficult to align the whole phantom precisely in a single B-scan, given that to align a single point (point target calibrations) is already difficult and requires a certain amount of experience and expertise. However, many variants based on the same mathematical principle have developed since. Beasley et al.[99] constructed the two-dimensional phantom using a ladder of strings with attached weights. Lindseth et al [82] proposed the diagonal phantom that is constructed with eighteen orthogonal wires forming a 3 x 3 x 3 grid. The nine crossings across the diagonal formed the two-dimensional phantom. Boctor et al [100] built the Hopkins phantom

with parallel wires in the shape of a cross. Leotta [81] used multiple coplanar wires with attached beads to assist in the alignment of the planar phantom. A reference bead is used with other line features in the image to segment the three reference points to be used to compute the calibration parameters.

<u>Z-Fiducial Phantoms</u>

The Z-fiducial phantom is designed to solve the difficult alignment problem . Wires are connected in a 'Z' (or 'N') shape as shown in Figure 3.5 (a). The probe is placed over the phantom and scans at an angle almost perpendicularly to the wires, producing three co-linear points in the ultrasound image, as shown in Fig. 4-7(b). Fig. 4-7(c) illustrates the mathematics of the ultrasound probe calibration. Each E1;E2;E3 and E4 is predefined in space. Hence the locations of the three lines forming the Z-fiducial are known. U1;U2 and U3 will be shown in the ultrasound image, and therefore the distances between them can be measure on the ultrasound machine. This means that each U_i can be located on line segments E_iE_{i+1}, and therefore in space as well. This gives rise to one independent constraint only, since the three points are linearly dependent. Hence at least three such Z-fiducials are necessary for calibration. The first article published with this technique for US described a phantom with only three Z-fiducials [74] that was actually made of small tubes instead of wires. Since then, the number of Z-fiducials has gradually increased to 30 [84]) increasing the registration accuracy. Lindseth et al [82] proposed a phantom with a pyramidal arrangement of Z-fiducials for curved-array probes (see sample US image in Fig. 4-7d). It also had a higher density of fiducials near the top of the image, so that, even when smaller depth settings were chosen, enough Z-fiducials were visible.
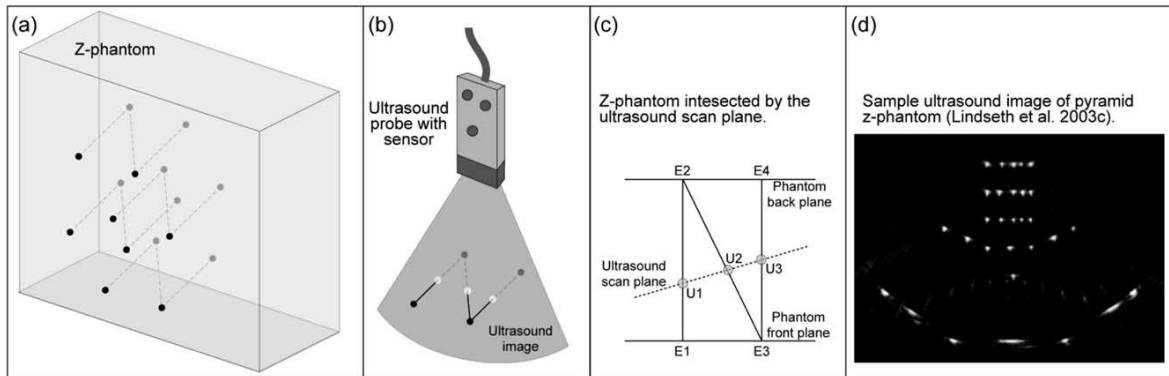
Fig. 4-7 Z fiducial phantom

4.2 Implemented method

Some trials has been performed using the different approaches reported before. At first it was experimental tried that single point calibrations methods are very difficult due to the inaccuracy in the determination of the points (cross wires were been implemented to perform tests).

Then the construction of a Z phantom using nylon wires was tried. Also this method appeared difficult to perform, the construction of the phantom was very elaborate. This type of calibration was abandoned. Finally a 2D alignment phantom has been realized. The phantom realized is an epoxy resin shape absorbed in a water tank. Four corners of the shape are located in space using a digitizer then these corners are segmented manually in the ultrasound B-scan, thereby solving for the spatial calibration parameters (Fig. 4-8).
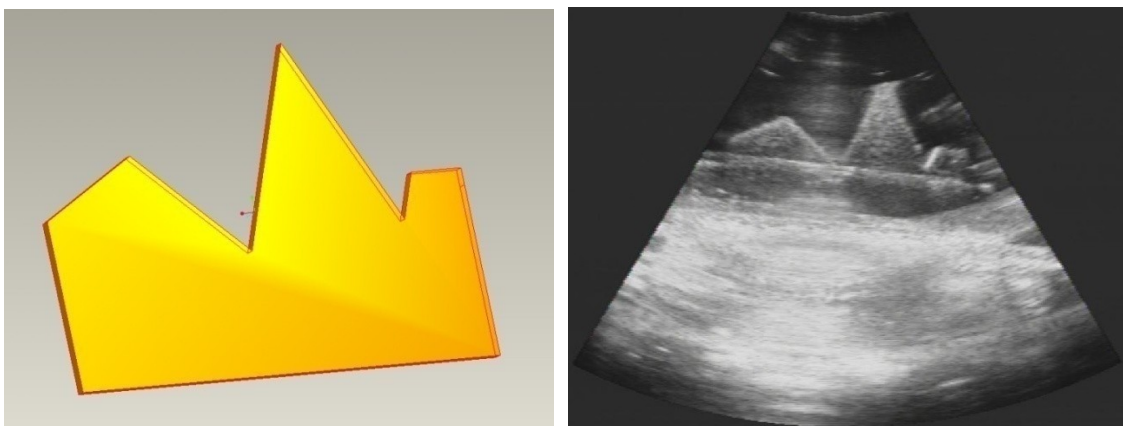

Fig. 4-8 2D Shape and US scan plane of the shape.

An C++ application has been developed. The ultrasound image are acquired in real time by means an frame grabber card. An graphical user interface has been developed (using QT library by Trolltech) in which in a 2D view the Us image is visualized. The user can selected the corners on this 2D View with the mouse. The data from the image and from the localizer are saved. Then offline a Matlab routine calculate the known transformation.

Good results were obtained but more than fifteen acquisition are necessary. It was decided to adopt a close form solution as shown in[101]. Then they were realized three identical 2D shape and fixed them to a thin plate, in different position and with different orientation.
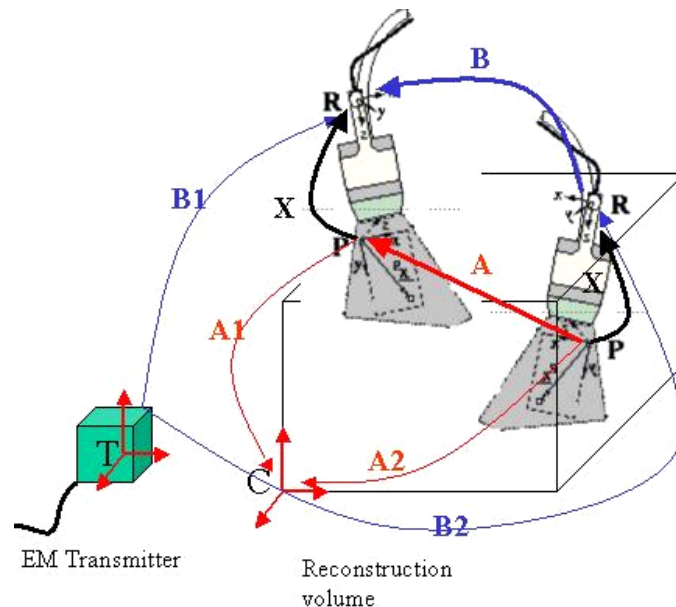
Fig. 4-9 Transformations involved in the calibration process in closed form

Fig. 4-9 presents the coordinate systems of the new formulation. A_1, A_2 are the transformations of US image coordinate system (P) with respect to the reconstruction coordinate system (C) at poses 1 and 2 respectively. From A_1, A_2, we have the transformation between US image coordinate system at pose 1 and 2, $A = A_2A_1^{-1}$. This transformation frame A, could be recovered using a calibration phantom to determine both A_1, A_2. B_1, B_2 are the tracking device readings for the sensor frame (R) with respect to tracker reference frame (T) at poses 1

and 2 respectively. Again the relative pose between sensor frame (R) at pose 1 and 2 is given by :

B = B2 $^{-1}$B1. This yields the following homogeneous matrix equation:

AX = XB

Where A is estimated from images, B is assumed to be known from the external tracking device, and X is the unknown transformation between the US image coordinate system and the sensor frame (R).

Using an optical pointer, 3D points of each of the shape are collected for offline processing. The 3D points of a shape are registered to the 3D points of the another shape to calculate the relative transformations between each pair of shapes($S_{1,2}$, $S_{1,3,}$ $S_{2,3)}$. This procedures should be performed only one time at phantom construction.

To determined the B and A matrixes the probe is moved until the scan plane is parallel to the thin shape. This is verified when the shape is completely shown in the Us image. The B matrixes are directly determined with two readings of the sensor when the probe move from the shape j to the shape i. To calculate the A matrix the user segments a point and a line on the shape. Then it is possible to calculate the transformation between the Us plane and the shape frame (T). Then for each pair (i,j) of shapes it is possible calculate:

A=T $_j$ $^{-1}$*$S_{i,j}$ *Ti .

The problem has been conducted to solve the equation

AX=XB

Then it is possible apply the same routine used to solve the robot calibration.

It is very difficult obtain a very precise calibration, for several reasons. The major source of expected error stems from the misalignment of the ultrasound probe to the plane of the shape. The Us beam has a finite

thickness then it is very difficult to pose the probe parallel to the shape. Further the corners of the shape in the Us image are not clear dot points but fuzzy and elliptic points. It was verified that the minimum error obtainable is about 3 mm.

5 Applications

5.1 Ultrasound guided robotic biopsy

5.1.1 Introduction

Minimally invasive percutaneous procedures under image guidance have a wide variety of applications in the fields of medical diagnostics and therapeutics. These procedures employ long, fine needles to access remote targets in the patient's body percutaneously. Biopsy and drug delivery are typical applications where these techniques are frequently used. Compared to equivalent clinical interventions performed under open surgery or laparoscopy, percutaneous needle punctures are fast, inexpensive, and minimize patient trauma. On the other hand it requires the localization of the target and of the needle trajectory using some forms of medical imaging technology. Among these technologies, the use of 2D ultrasound is common because of its minimal equipment requirement and real-time visualization. In practice, the target, such as a lesion suspected of being cancerous, may reside deeply within the body and may be adjacent to organs and tissues sensitive to injury. This makes precise needle placement of critical importance, but such precision is generally difficult to achieve in free hand procedure execution. The combination of poor image quality of the ultrasound images, their two-dimensional limitations and the flexibility of the needles used in these procedures, determine frequently many trajectory adjustments for the target reaching and sometimes the physician cannot conclude the procedure with the consequence big waste of time and stress for the patient. For these reasons the success of ultrasound guided interventions deeply depends on the clinician's abilities and requires very long training and particular manual and mental 3D reconstruction capability for the planning of the needle trajectory and the execution of the procedure. In the last years some technological aids have been developed to enhance the accuracy and to minimize the ability dependence using navigation system and/or robotic systems.

In[1] Cleary et al. present a review of four interventional robotics systems: the AcuBot for active needle insertion under CT or fluoroscopy, the B-Rob systems for needle placement using CT or ultrasound, the INNOMOTION for MRI and CT interventions, and the MRBot for MRI procedures. A lot of works have been developed on robotic system for transrectal [2] and transperineal biopsy of the prostate with ultrasound guidance[3]. A robotic tool with an automatic image-guided control based on "visual servoing" is presented in [4] and [5]. On the other hand several navigation system for percutaneous interventions have been the subject of studies [6]-[9]. Fitchinger et al.[7] introduced an image overlay system to assist needle placement with CT scanning and Khamene et al. [9] showed an approach to biopsies performed using a 3D augmented reality guidance system with the using of Head Mounted Display (HMD). Commercially there are some navigation systems for percutaneous intervention, such as the Traxtal PercuNav [10] available in United States, Esaote Virtual Navigator [11] and Hitachi Real-time Virtual Sonography [www.hitachi-medical-systems.eu].

The first integrated systems that offers both navigation functionalities and robotics [12]-[15] have emerged in recent years. In[15] Boctor et al. propose the use of a dual robotic arm system that manages both ultrasound manipulation and needle guidance and a navigation system based on 3D Slicer (http://www.slicer.org/).

The proposed solutions are often too complicated and they cannot be applied for abdominal organs due to their movements.

Analyzing clinicians at work during the execution of manual US guided percutaneous biopsies, it is clear that the difficulty resides in the correct orientation of the needle to reach the target. In some cases clinicians can use a mechanical aid. For this cases clinicians can use needle guide to fix on the US probe with a known angle of the needle trajectory in the image plane. Many US scanners offers similar needle guide and in

some cases they allow to show over the image the known needle trajectory(Fig. 5-1).

Fig. 5-1 Esaote needle guide

When the needle cannot be inserted on a fixed trajectory along the US scan plane, often, in particular for not experienced clinicians, it is difficult to reach the target. It is very difficult to imagine the right trajectory to guide the needle on a point that lies on the US scan plane inside the patient body. The clinician has to localize in 3D in his/her mind the target visualized on the US screen. It is possible since the clinician see where the US probe is positioned and so he/she can imagine the scan plane inside the patient, than watching the 2D image he/she have to right position the target on the plane. After that the clinician have to obtain a needle trajectory to reach the planned point inside the patient. A very difficult task that require high clinician orientation and manual abilities. For this reason it has been the system [22] based on the combination of the advantages of virtual reality and robotics in one integrated system. The idea is to provide the clinician an mixed reality system, that allows to plan accurately and easily the

trajectory and intra-operative helps him to execute the procedure, and a robot that allows to obtain the necessary precision. The system is designed to provide great accuracy, while keeping the biopsy procedure simple and intuitive:

- the clinician has only to select the biopsy target directly on the US image, using the mouse, and a skin entry point on the patient's body, using a digitizer. Subsequently, the robot positions the biopsy needle handler along the trajectory defined between these two points. In order to guarantee maximum safety, the insertion of the needle and the bioptic sampling is left to the manual execution of the clinician. An interactive graphical interface is provided to the surgeon with a 3D virtual scene where the optically tracked needle and probe and the relative scan plane are shown in real time beyond the traditional 2D View of ultrasound scan. A 3D model of anatomy reconstructed from precedent CT dataset can be integrated and visualized in the virtual scene. In order to compensate inaccuracy due to patient's motions or needle deflection we implemented a surgeon-robot cooperative control by means of a force/torque sensor. In this manner the robot, after the planned position achievement, follows the surgeon's movements allowing a fine adjustment of the needle trajectory in a natural manner during the needle insertion.

5.1.2 Methods and Instruments

A.   Hardware Design

The setup of the system, represented in Fig. 5-2 consists of an ultrasound image system (Au3 partner, Esaote Biomedica) equipped with a probe (Esaote 3.5 MHz CA11), an industrial 6 Degree Of Freedom (DOF) Robot Samsung ATI 2 with servo-controller, an localization system (Optotrak Certus, Northern Digital Inc.) and 2 Personal Computers (PC). The image guided system and the graphical user

interface are implemented on the first PC (PC1), while the cooperative control of the robot runs on the second one (PC2). The robot is equipped with a mini-45 Ati force/torque sensor (www.ati-ia.com), which is used as input data for the surgeon-robot interaction controller.
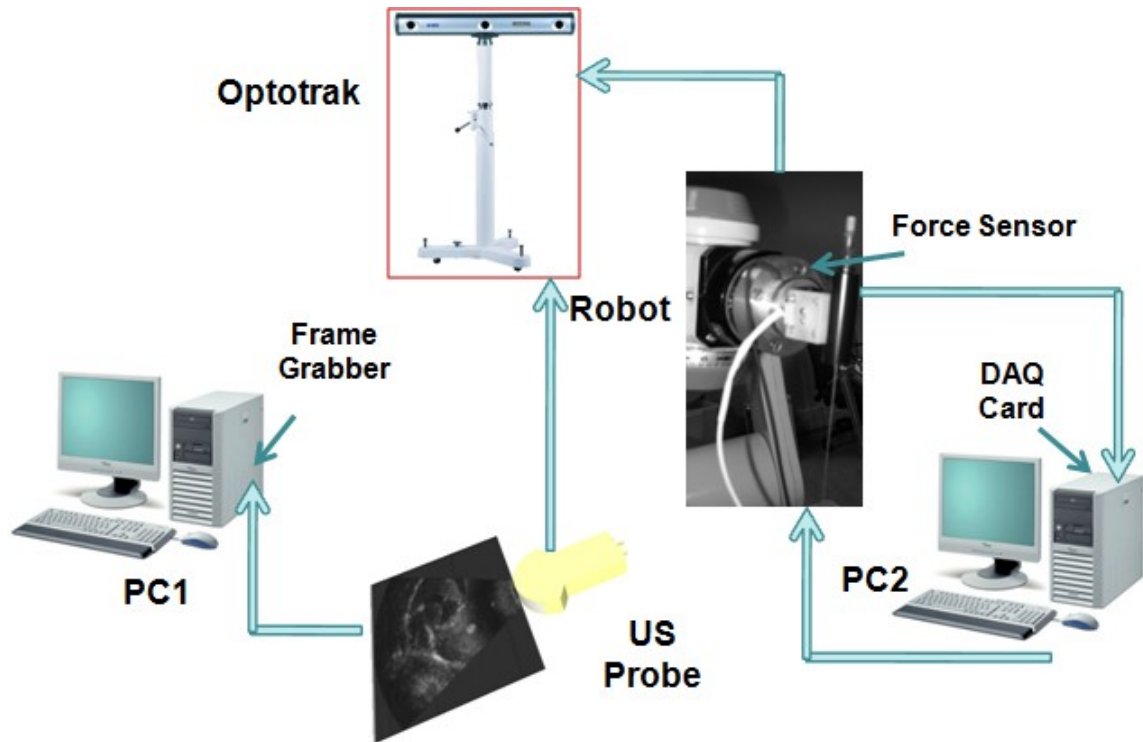

Fig. 5-2 Overall Set-up of the sytems

The needle is handled by a holder fixed on the force sensor, which is attached to the robot wrist. This holder has been realized following two stages of design in order to find the most useful solution. The first prototype has been designed and manufactured as a 1 DOF mechanical slide. It is composed by two parts: one is fixed to the force sensor and then to the robot, while the other one is the effective slide which has been designed with the right tolerances to improve sliding without falling. Thanks to its geometry and to the boundary conditions created, this guide allows a stable insertion into soft tissues minimizing deflections of the needle. A second version of the holder prototype has a small cylindrical hollow handle Fig. 5-3 to improve ergonomics when the robot is in shared-control modality. Both versions are equipped with

infrared leds for the 3D localization of the end-effector in the space of the intervention.
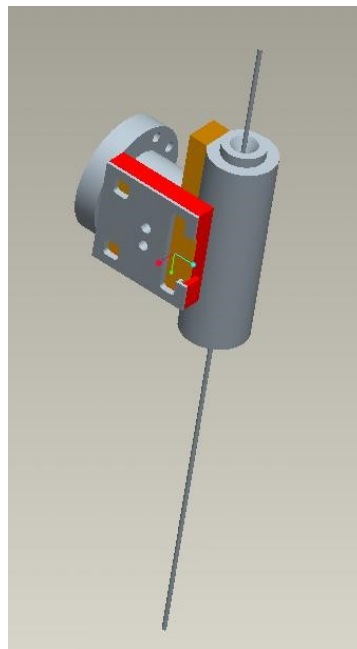

Fig. 5-3 Needle holder

Calibration of the System Components

The localizer is used to acquire and refer all geometrical relations, involved in the system, in the same reference frame by means of sensors placed on the instruments. The calibration of the ultrasound and of the robot have been addressed in the previous chapters.

In image guided medical applications involving tools attached to a robotic arm, it is essential to be able to accurately localize these tools in the robot end-effector frame. Then another necessary calibration is that of the needle. The objective is to pose the needle tip at a planned point with a planned orientation. It was fixed the needle frame with the origin on the tip and the z axis parallel to the needle axis. The unknown transformation was calculated acquiring three times the needle tip at different level of insertion in the holder, using a pointer with a surface planar with a divot at center, where easily it is possible insert the needle tip. This matrix of transformation T_{needle} is applied to the 3D virtual model of the needle and it used to move correctly the robot

when it is under cooperative control. Another transformation matrix that is necessary calculate is that between the force sensor frame and that end-effector frame. This matrix depend by the sensor mounting and it was calculated mechanically by performing some measures.

Software design

Two software applications have been developed: the first one that implements the image guided system running on the PC1 and the second one that implements the clinician-robot cooperative control running on the PC2.

Control Software. The can be in two modality of functioning : *Preprogrammed, semi autonomous motion:* The robot is under position control. Based on the target and skin entry point location the robot moves to the desired position with the appropriate orientation. A second position control loop in the global reference system has been implemented by means of the localizer to minimize the position error. The industrial robot have a high repeatability, but not a high accuracy. This controller is embedded in the image guided system running on the PC1. This additional control loop allows to obtain a maximum positioning error of 1 mm.

Cooperative control : after the desired position and orientation is reached, the clinician switches to "cooperative control" modality, the robot follows the surgeon movement.

The cooperative control software is implemented in C++ language and runs on PC2. This application can be divided in two main modules: the acquisition module and the control module.

Acquisition module
This module manages the force sensor. The force signals are read by using a National Instrument PCI_6026E (www.ni.com) data acquisition card with a sampling time of 1ms.

It was necessary filter the signals because the signals were highly disturbed by the noise due the robot motors. A second order digital Butterworth filter was implemented.

Control module

This module implements the cooperative control law and manages the communication with the robot low level controller.

Cooperative control

In a cooperative system the human operates "in-the-loop" with the robotic system. The surgeon grasps the tool held by the robot or a control handle. A force sensor senses the direction that the surgeon wishes to move the tool and the computer moves the robot to comply. Two robot control paradigms commonly used in human-machine systems: admittance and impedance control. Hashtrudi-Zaad and Salcudean provide a comparison for the two control paradigms for a teleoperator [46]. In general, admittance-controlled robots are non backdrivable, have highly-geared motors, and are equipped with a force/torque sensor. The robot velocity is proportional to the user's applied force as measured by the force sensor. Admittance control, together with the stiffness and non-backdrivability of the robot, allows for slow and precise motion. Examples of clinically-used coooperative robots include the LARS [106], the Johns Hopkins Steady-Hand Robot [105], the Acrobot (Active Constraint Robot) [52, 27, 28]. The Acrobot works cooperatively with the surgeon to guide him/her during bone cutting for knee surgery. The LARS and the Steady-Hand Robot are admittance-controlled robots.

In this work was implemented an admittance control law: the robot movement is proportional to the exercised forces:

$x = Kf$

where x: 6x1 position and orientation vector; K: 6x6 diagonal matrix; f: 6x1 force and torque vector.

This type of control was inserted to implement a fine adjustment of the trajectory to overcome to needle deflection and target moving problem. Only small movements are necessary. The movement should be performed respecting the fixed point at the skin entry point (end of the needle holder). The movements are referred respect to a needle frame with the z axis parallel to the needle axis. Only the two rotations pitch and yaw are considered. This type of control is not safety because the low level control of the industrial robot is a position control then it sure that at the end of the movement the needle has the planned orientation and fixed position it maintained but it can assume any position during the movement. This type of problem is solved in literature using two type of approach. The first approach uses a passive wrist to allow in general the tool to pivot around the insertion point and has been used in the commercial Aesop and Zeus robots as well as several research systems. The second approach mechanically constrain the motion of the surgical tool to rotate about a remote center of motion (RCM). Usually the robot is positioned so that the RCM point coincides with the entry point. This approach has been used by the commercially developed da Vinci system as well as by numerous research group, using a variety of kinematic design [1].The tasks of 3D needle orientation and needle insertion is mechanically de-coupled using a remote centre of motion design. With the RCM design, a single point in 3D space acts as a pivot point for the orientation of the needle and is also intended to correspond to the needle insertion point. This design is advantageous for intra-cranial interventions, as the path of the needle will always be constrained to pass through a small bore drilled in the skull. RCM designs also offer the advantage of being able to compensate for tissue deformation and needle deflection by steering the needle about a fulcrum point during needle insertion [102-103]. While the RCM idea has made significant impact on the field, it has some disadvantages: (1) precise construction must guarantee the existence of a known fulcrum point, (2) a tool holder must be carefully designed for each new tool, placing it exactly on this fulcrum point, (3) each joint must be fully

encoded, and (4) the kinematic chain must be a priori known. The net result of these factors is a complex and expensive structure that must be carefully designed, manufactured, and calibrated .An alternative to constraining the fulcrum point mechanically is to generate a programmed, or "virtual" RCM in software using precise kinematic (and in some cases, dynamic) models of the robot. By modeling the dynamics of the robot using the operational space formulation [2], partitioned control [7] can be used to alter the behavior of the system to appear, kinematically and dynamically, to be an RCM device. Boctor et al [104] proposed a programmed-RCM robot with an Artificial Intelligence based search optimization, resulting in a rapidly converging motion algorithm for needle placement that does not require either encoded joints or complete knowledge of robot kinematics. In this work this problem it is not addressed at the moment.

Image guidance.

Starting from the EndoCAS Navigator platform, it was developed an image guided system with the functionalities necessary for ultrasound guided biopsy. In this study were not treated the generation of virtual patient specific models and their registration, this modules were imported by the platform.

The system designed visualizes in a 3D virtual scene with patient-specific virtual anatomy, the real time position of the ultrasound probe (with its 2D image), the target position, the selected entry point, the calculated trajectory and the instantaneous pose of the real needle (Fig. 5-4).
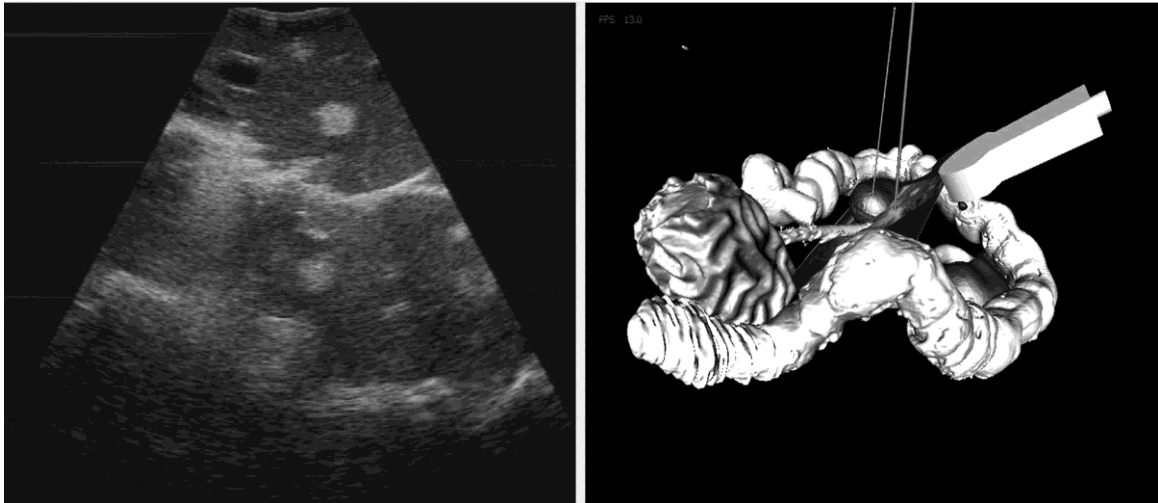
Fig. 5-4 2D ultrasound scan plane and 3D rendered scene

In addition there is a conventional 2D window for the visualization of the ultrasound image where the surgeon selects, using the mouse, the target point of the procedure. Whereas the entry point on the skin is acquired using a digitizer. To realize and render the 3D window it was use Opensg based on scene graph.

Two type of localizer were integrated the optical Optotrak and the Aurora. The user can choice by means the GUI the type of localizer to use.

5.1.3 Results

At first the system has been evaluated by non expert physicians in free hand biopsy procedures. To assess the performance and the accuracy of the system two types of experiments have been conducted. A first set of experiments have been made to test the global accuracy of the needle placement that depends on the several calibrations (robot, ultrasound probe, and needle) performed. The error was characterized in ideal rigid conditions using a home-built phantom composed of three peas of different diameter (10, 8 and 6 mm) of agarose (3% solution) positioned in a water tank. The goal of each trial was the insertion of the needle inside the selected pea after the selection of its centre as target, without manual correction on the orientation of the needle holder proposed by the robot and without patient-specific virtual

anatomy models. Ten trials have been made for each pea. The results are shown in table 1. The reaching of the pea indicates that the positioning error of the needle is lower than the radius of the pea.

TABLE I
GLOBAL ACCURACY OF THE NEEDLE PLACEMENT

Pea diameter	N°. trials	% Success	Error
10 mm	10	100	< 5 mm
8 mm	10	100	< 4 mm
6 mm	10	60	< 3 mm

Table 1

A second series of experiments have been performed to evaluate the usability of the cooperative control for the compensation of needle deflection, deformation of tissue and target movement. For this type of experiments we used a tissue like liver by Kyoto Kagaku (www.kyotokagaku.com), which intrinsically determines the above mentioned errors. Further an additional random error was introduced moving the surgical bed of few centimeters after the selection of the target (simulated tumors present in the phantom) and the trajectory planning. In this way the user cannot reach the tumor with the only insertion of the needle. Then the cooperative control is activated, in this modality the robot follows the user movements, the user can adjust the orientation of the needle in a natural way (as in a freehand biopsy). The user can select again the target on the ultrasound image, then the new trajectory is visualized in the 3D virtual scene, allowing the user to place the needle for target reaching more easily. Thirty trials were performed by 3 non expert users. In all cases the user was able to place the needle for target reaching (verified on the ultrasound image).

5.2 A Mixed Reality Navigation Guidance for HIFU treatment

High Intensity Focused Ultrasound (HIFU) represents a therapeutic application of ultrasound technology for the treatment of solid tumors and for hemostasis and other vascular diseases in human tissues. HIFU is a percutaneous thermoablation technique based on the ability of collimating ultrasound energy through a lens in a focal region to achieve the cell death by coagulative necrosis. HIFU works with a range of frequencies within 0,8-1,6 MHz with an intensities of the order of 10 KW/cm² into the focal region. This huge amount of energy, focused on a restricted area of tissue, provides two different type of biological effects: thermal and cavitation. The absorption of the acoustic energy in the focal region tissues implies an increasing of temperature, up to 60°C or higher, enough to burn the cells. Cavitation is a mechanical effect due to alternative phases of compression and expansion of tissue molecules resulting in continuous bubbles formation and collapsing, which provide disruption of cell membranes. The combination of all these two effects determines cell death by coagulative necrosis, rupture of cell membranes and apoptosis without, or minimized damages, to tissues outside the focal region. Although the possible use of high intensity ultrasound generated by an extracorporeal source for therapeutic purposes had been investigated since the 1940s, the real development and application of this procedure, as it is up to date, have been conducted over the last two decades especially in China, where HIFU was born, and other Eastern countries including Japan in which this technique has been widely applied (more than 8000 treatments from 1997 to 2006).

Several clinical studies have been conducted over the last 10-15 years by different research groups worldwide to test out every potential application of HIFU and most of these investigations have confirmed the effectiveness and safety of the procedure in many features and fields. The main indication, and probably its most interesting and challenging

topic among HIFU's clinical uses, is treatment of solid tumors, either benign or malignant, primary or metastatic [105-109]. For early-stage neoplasms, and especially for primary localizations, other applications which have been tested and reported in literature include: arterial occlusion for both bleeding or tumor treatment thrombolysis, hemostasis of vessels and organ's bleeding, drugs delivery[110].

To guide a HIFU therapy it is necessary an imaging device for targeting and monitoring the treatment site. Currently, for this purpose are used MRI guidance (in ExAblate system by Insightec and in Sonalleve by Philips systems) and ultrasound guidance (in Haifu by Chongqing Technology Co. Ltd. and HIFU-2001 by Sumo Corporation Ltd systems). The two machine available for intracorporeal prostate treatment (Sonablate by Focus Surgery, Inc., Ablatherm by EDAP TMS) use ultrasound guidance, too.

The MRI guidance allows a better visualization and identification of the treatment zone because of high quality of images and 3D patient anatomy representation but it is expensive and requires dedicated equipment and location (mainly due to the large footprint and in particular the high magnetic field involved). Although ultrasound imaging does not provide detailed and clear images and offer just a 2D slices of the anatomy, it has the ability to obtain simply, quickly and cheaply useful guidance information.

The machinery availed in our HIFU centre inside Cisanello Hospital in Pisa is the latest JC200 therapeutic system Haifu (HIFU) by Tech Co., Ltd, Chongqing. It essentially consists of an ad-hoc designed tilting bed (Fig. 5-5) equipped with an ultrasound therapeutic transducer (targeting transducer depicted in Fig. 5-6), able to generate a high intensity ultrasound beam through the above lens, it is located in the centre of the treatment table into a reservoir automatically fillable with degassed and distilled water that acts as coupling medium between the transducer itself and the patient's body; a conventional diagnostic

ultrasound probe (localization probe), that allows a real-time localization of the lesion to treat, it is integrated in the centre of the targeting transducer, so that the localization probe and the targeting transducer are coaxial and joined; a Cartesian motion device (HIFU motion device) able to smoothly move the localization/targeting system with millimetric precision moved by the operator who sits at the console provided with a monitor for the target localization on the US images and a control unit. The localization probe, in addition to the three translations of the localization/targeting system, has an additional rotational DOF (Degree Of Freedom) around its main axis used to better visualize some regions.

The experience in Pisa has highlighted advantages and limitations of the HIFU system. Although it offers tremendous potential for noninvasive treatment of malignancies, HIFU has limitations due to general anesthesia and long time required to perform the procedure as well as the difficulty to find sometimes a good acoustic window because of bone or gas interfaces and respiratory motion artifacts which can even preclude procedure performing. Furthermore, lesions that are clearly visible during a traditional ultrasound examination, are sometimes difficult to detect with the localization probe integrated in the HIFU system.

This is mainly due to: 1) Movement limits of the localization/targeting system. The system has 4 DOF for the probe and one for the patient (tilting bed) moved by the operator at the console control unit. The independent and remote management of the degrees of freedom does not allow a natural localization of the target and also the offered limited range of motion requires often the (manual) repositioning of the patient. 2) Orientation difficulties using the location/targeting system, which is unnatural for doctors in respect to traditional freehand ultrasound, due to the inability to see the probe (drowned in the tank inside the bed) respect to the patient. Although the graphical user interface shows a schematic of the probe and the patient, the doctor

76

often "loses itself" and takes a long time to locate the treatment area. In order to reduce many of the previous troubles it is necessary other source of morphological information that allow to better find and localize the target to burn.

It was developed a navigation system with the aim to overcome these limitations and then to increase the number of possible treatments and to reduce the times of sittings and the risk of potential errors.

5.2.1 Methods and Instruments

The image guided system [21] has been designed using an additional imaging system coupled with a localizer. The system has been integrate in the HIFU system to allow an easy target localization. Among several types of imaging used to integrate the HIFU location/targeting system, including MRI and CT, an additional traditional ultrasound to use freehand is a good choice because: it allows to identify clearly and simply the treatment area, as demonstrated by the fact that is often used to plan the treatment (before the treatment itself). Its integration with the HIFU system, as described below, requires no changes to machinery and requires no special spatial needs (such as MRI and CT).
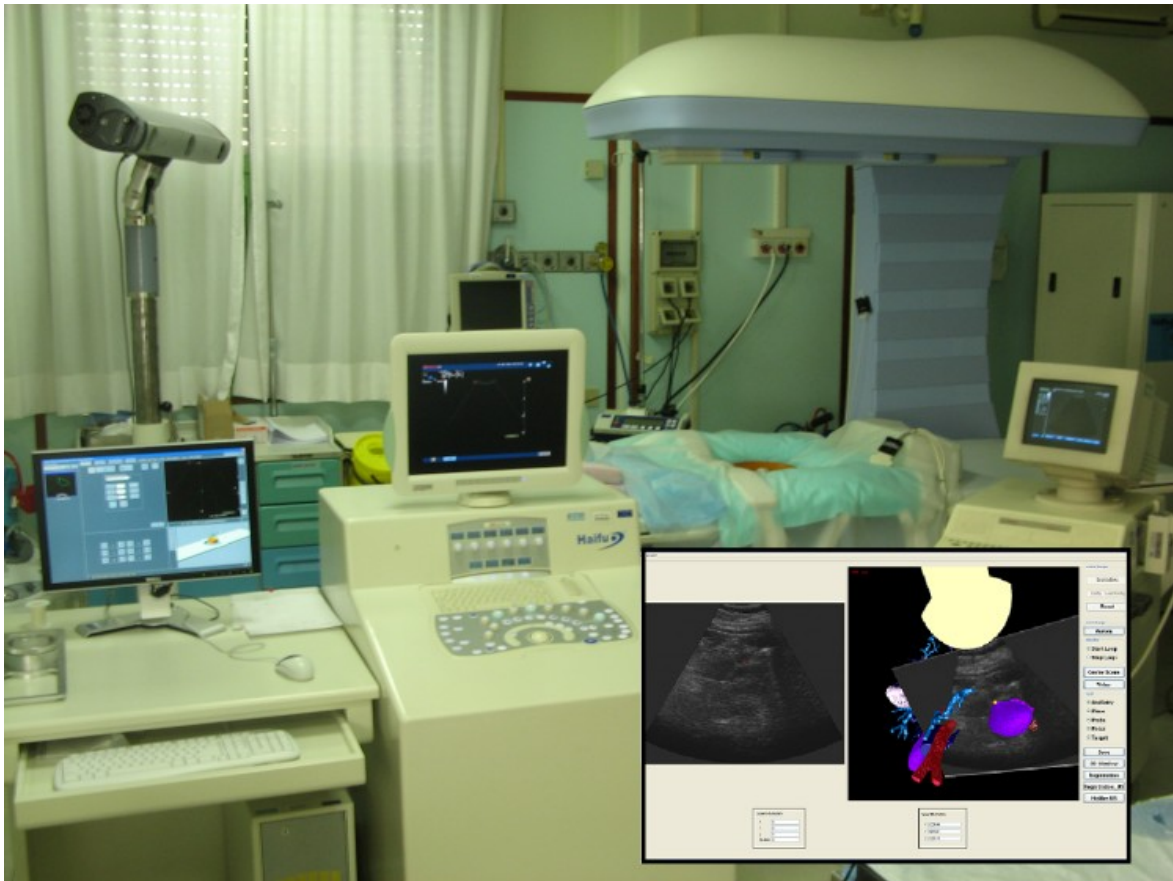
Fig. 5-5 Set-up of the HIFU navigator system

In addiction it is always possible to use pre-operative CT or MRI images as an additional source of information for the operator.
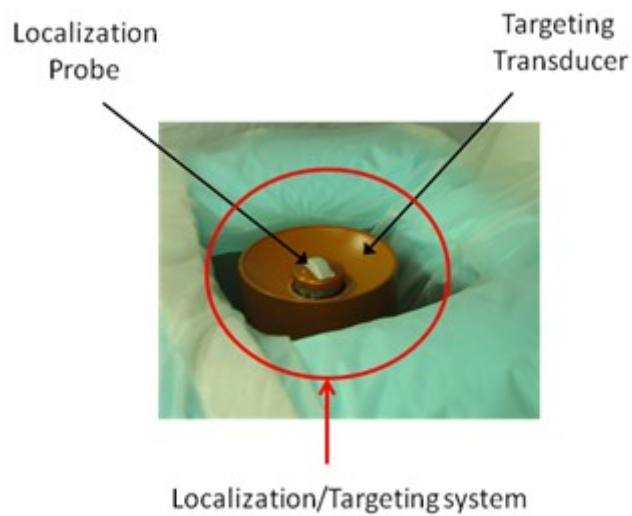

Fig. 5-6 Localization/Targeting system of the therapeutic system Haifu (HIFU)

Following this considerations we developed a navigation system that shows to the clinician, in real time, in a 3D virtual scene: the patient-specific virtual anatomy, reconstructed from CT radiological images, the additional movable ultrasound probe, the US 2D image instantaneously projected on the current US scan plane, and the HIFU focal point. It will also provide the classical 2D ultrasound image visualization. In this manner the clinician can localize more easily the target zone using various approaches. He /she can search the target using directly the additional freehand ultrasound probe. He/she can view the current position of the US scan plane in respect to the (virtual) patient anatomy and in respect to HIFU focal point. Eventually, if the target is not visible by the additional ultrasound probe, for example due to patient decubitus, he/she can localize the zone to treat using just the virtual anatomy. The user can select the target zone clicking on the scan plane of the additional ultrasound probe, or directly on the CT images.

The system indicates how to position the HIFU localization/targeting system to reach the target zone. Then the clinician can verify the target location using the traditional localization probe (mechanically aligned with the targeting system) and accurately plan the zone to burn searching the lesion borders slowly moving the localization/targeting system. The implemented image guided system has some functionalities as those the biopsy system described in the previous chapters. The setup of the system, represented in Fig. 5-5 , consists of an ultrasound image system (Au3 partner, Esaote Biomedica) equipped with a probe (Esaote 3.5 MHz CA11), the JC200 by Haifu (HIFU) Tech Co., Ltd, Chongqing (China), an optical localization system (Optotrak Certus, Northern Digital Inc.) and a Personal Computer (PC) equipped with a frame grabber card (Picolo Alert by Euresys) to acquire the video by the ultrasound machine. The design and implementation of navigation systems requires solving several basic problems: localization, calibration, virtual anatomy representation, registration,

design and implementation of the Graphical User Interface (GUI). In the following paragraphs they are described in details our ad-hoc solutions for the HIFU navigation system.

A. Localization

The localization system allows real-time tracking of the position and orientation of system components, required for a coherent representation of the information to offer the clinician (using virtual and mixed-reality techniques). It was chosen an optical localization device (Optotrak Certus, Northern Digital Inc.). It was tried an electromagnetic localizer (NDI Aurora, Northern Digital Inc.), but it is not compatible with the HIFU machine (probably because there are too much ferromagnetic components around the HIFU parabola). The using of an optical localizer allow high tracking precision but can introduce some limitations for the clinical staff, which have to guaranty sensors visibility (not required for electromagnetic devices).

The localizer allows to acquire and refer all geometrical relations, involved in the system, in the same global reference frame (Clinical Space) by means of optical sensors placed on the additional ultrasound probe and on the HIFU machine. Sensors positioning have been studied in order to guaranty their visibility taking into account the location of the clinical staff in the HIFU room.

Fig. 5-7 optical sensors fixed on the HIFU machine and ultrasound probe

<u>B. Calibration of the system components</u>

The localizer acquires the location and orientation of the sensor placed on the objects, respectively the additional US probe and the HIFU machine, rather than the ones of our interest, respectively the US scan plane and the HIFU motion device. The ultrasound probe calibration has been addressed in the chapter 3.

To place the HIFU device focal point in a precise 3D point of the Clinical Space, it is necessary to determine the geometric relation between the HIFU motion device reference frame and the optical sensor frame fixed on the HIFU machine (HIFU reference frame). To perform this calibration we have used a simple method. an infrared led was put on

the localization transducer (coaxial to the treatment transducer) of the HIFU machine. Then localization/targeting system has been moved the by means the motion device along the three directions x, y and z. The movements have been acquired by the optical localizer and then it has been possible determine the rotational part of the transformation matrix between the HIFU reference frame and the HIFU motion device reference frame. The translational part of the transformation matrix was calculated determining the centre of the circumference obtained by points acquired moving a digitizer along the circular ultrasound probe. This calibration allows to transform the target point expressed in the Clinical Space in the motion device reference frame. The total transformation chain to apply to a selected target to obtain the coordinates of movement to impose at the HIFU machine, is showed in the following figure.
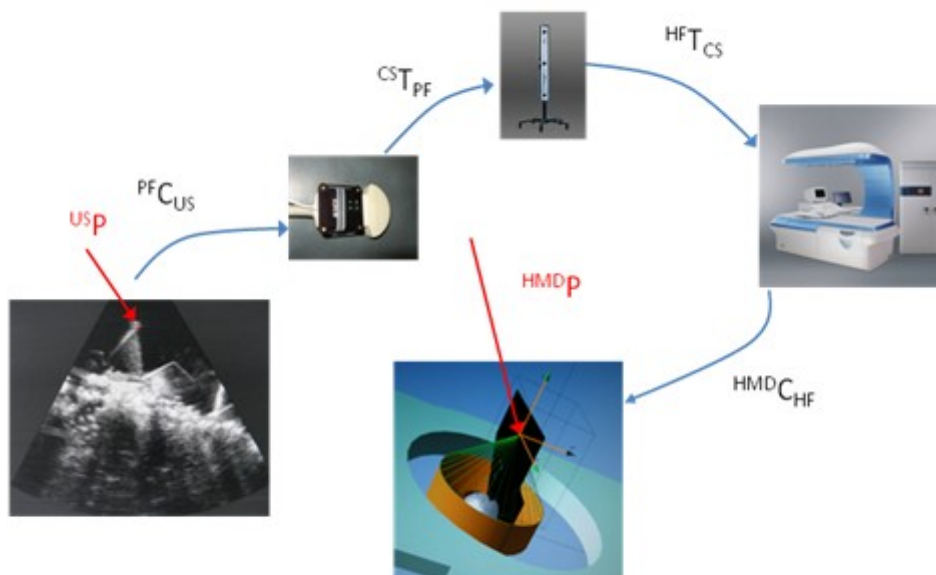
$^{PF}C_{US}$: Calibration matrix representing the transformation from ultrasound plane reference frame (US) to US probe reference frame (PF);

$^{CS}T_{PF}$: Transformation from US probe reference to Clinical Space reference frame (CS);

$^{HF}T_{CS}$: Transformation from Clinical space reference frame to HIFU reference frame (HF);

Fig. 5-8 Transformation chain from selected point target from US reference frame up to HIFU motion device reference frame

For the virtual anatomy representation, a surface rendering was adopted, for the segmentation and rigid registration were imported the module developed in Endocas navigator. In particular the registration is performed in two steps. A first it is performed a roughly registration based on external artificial markers placed on the patient skin. In particular three radio opaque fiducial markers were attached on the patient external surface in correspondence of the sternum (one marker) and of the iliac spines (two markers). Fiducial markers baricentres are acquired in the CT reference frames and registered with the corresponding points acquired before the treatment on the patient, positioned and fixed on the bed, in the Clinical Space using a digitizer.

This type of registration is not sufficient for abdominal soft tissues in particular because the CT data are acquired, for diagnostic purposes, in supine position, while the treatment is often performed in lateral or prone decubitus. It determines a relative displacement (due to gravity) between virtual patient (obtained by CT data) and the real anatomy (the patient).

To refine the alignment a second registration is performed using internal anatomical reference points, close to the target zone. In this case the couple of reference points are acquired using the localized ultrasound images on the patient and determining the coordinates of the corresponding points on the CT data[111]. This registration can be repeated whenever necessary. This allow to obtain a more precise matching between intra-operative and pre-operative data in the treatment zone.

5.2.2 Results

The first in-vitro experiment was performed in the EndoCAS laboratory to test the ultrasound calibration and the anatomy registration. An pig spine model extracted by a CT dataset and printed, in ABSplus material, by means of a 3D printer (Elite by Dimension) was place in a water tank. Three landmarks on the spine were selected with a digitizer

in the Clinical Space reference frame. The same landmarks were acquired in the CT reference frame. The model registration was performed. The accuracy was checked by selecting distinct points with the mouse in the US plane and verifying the relative location on the 3D mixed reality scene on the GUI. In all cases the accuracy appeared to be in the order of magnitude of few millimeters (maximum 2 mm).

A second in-vitro experiment was performed to test the accuracy of the system calibration of the entire transformation and calibration chain in the HIFU treatment room. A pig spine model was placed the inside of the HIFU tank full of water, the relative virtual model was loaded and registered to the real one. A point of the model was selected on the US images as target then we command to HIFU motion device to move to the location suggested by the navigation system. After the movement, the accuracy was verified on the US Image of the GUI console of the HIFU.

The trial was repeated 25 times changing spine position. The difference between the focal point and real target, chosen by the clinician on the US plane, appeared to be less than 5 mm. A first simulation experiment using a volunteer was performed to test the efficacy of the navigation system. The aim of this experiment was to target a point inside the liver. We attached on the patient abdomen three radio opaque fiducial markers in correspondence of the sternum and of iliac spines before subjecting the patient to CT. They were segmented by the CT dataset some organs of interest such has liver parenchyma, kidneys, gallbladder, abdominal aorta, cava vein, etc. Then we reconstructed anatomical structures surfaces to load in the HIFU navigation system. Then, on the HIFU bed it was performed the registration between the 3D virtual anatomy and the real patient, acquiring the digitizer position in correspondence of the markers. A clinician expert in ultrasound diagnosis used the system. It verified that really there was a misalignment between the anatomy show by the ultrasound probe and the virtual anatomy.
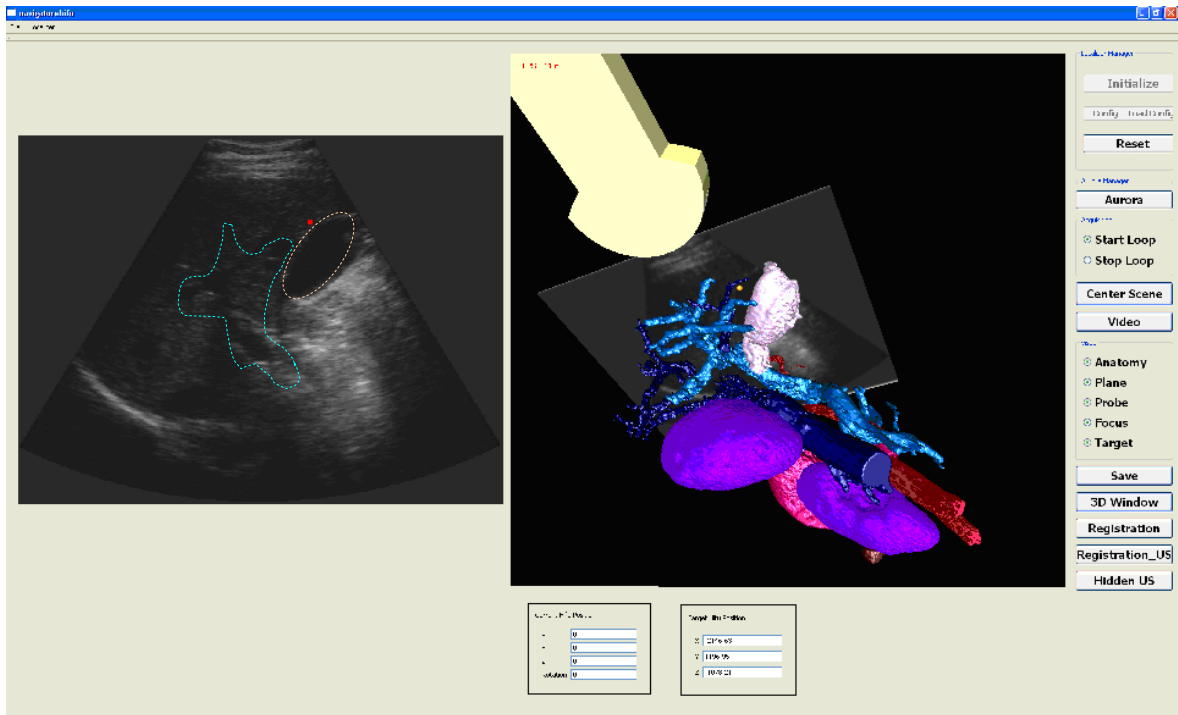
Fig. 5-9 Correspondences between anatomical structures on the US image (left) and on the 3D virtual scene (right). The highlighted structures on the US image represent the portal vein and the gallbladder

A registration refinement was performed. The sonographer selected the bifurcation of the mesenteric artery in the splenic and hepatic artery, superior pole of right kidney and the bifurcation of the portal vein for the left and the right liver lobes.

The same points were determined in the CT reference frame, then we performed the ultrasound base registration aligning the two points clouds. After this second registration we obtained an acceptable alignment.

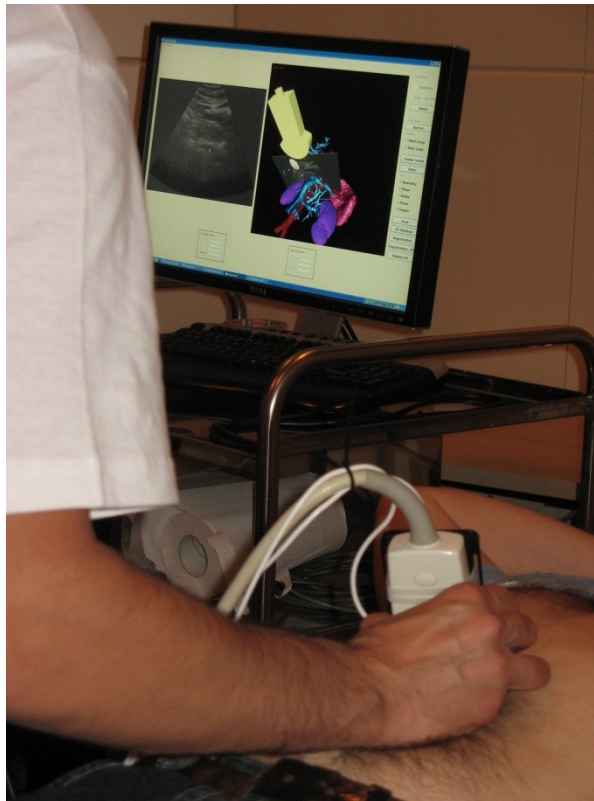*Fig. 5-10 A clinician is trying the US navigation functionalities*

Two clinicians tried the navigation system and evaluate it very positively considering the system very useful to help the clinician to orient in the 3D space. Some screenshots of the system are shown in Fig. 5-9 and Fig. 5-10 and in Fig. 5-11. They highlighted the correspondence between points on the 3D model and on the US image.
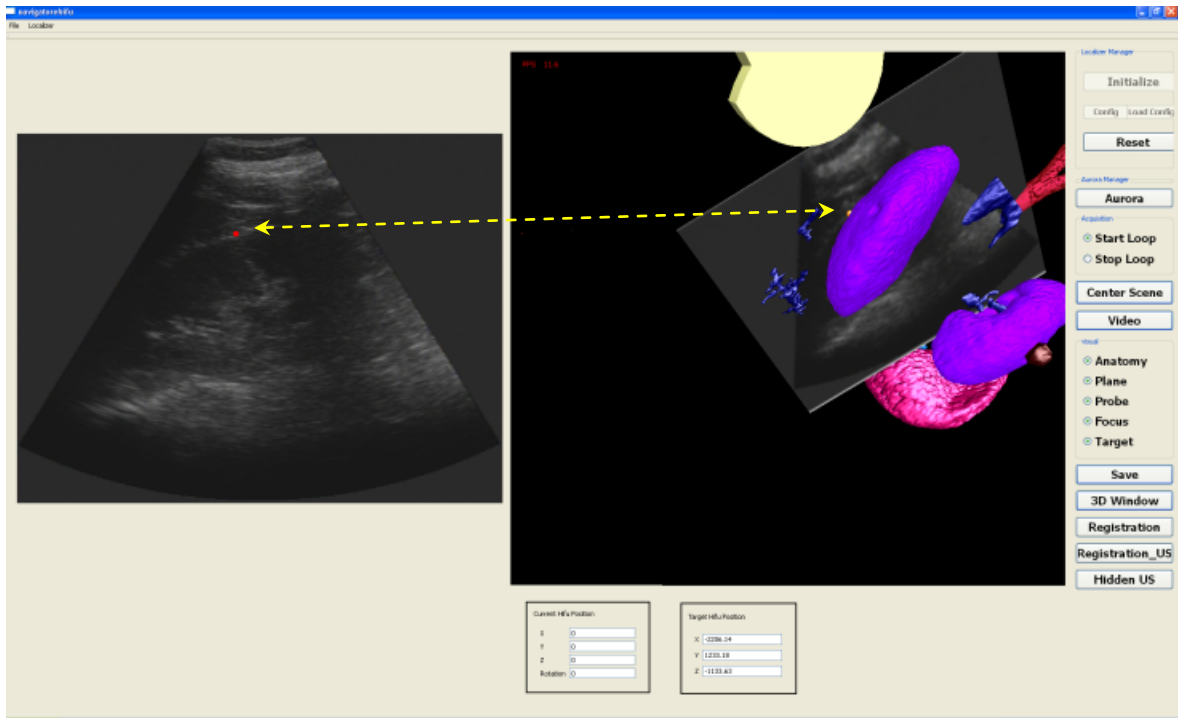
Fig. 5-11 The red point on the US image selected on the kidney parenchyma border (left) corresponds to the point in the 3D virtual scene (right)

Part III Conclusion

This thesis demonstrates feasibility and potentialities of the introduction of robotics and image guidance in the overall, in particular in the phases of diagnosis and treatment.

The increasing use of robots in the operating room, above all the da Vinci surgical telemanipulator, as demonstrated in the technical review (chapter 2), shows that this technology is valid and accepted and encourage on one hand to improve existing systems and on the other to explore new fields of application for robotics in the clinical field.

This study demonstrates the potential use of anthropomorphic robots and image guided systems for the diagnosis and treatment of tumor. Robots can be easily integrated in the traditional clinical scenario, to obtain smart functionalities, by means of a localizer and calibration routines. The algorithms and methods developed can be easily adapted to each anthropomorphic arm. In this way this work can be integrated with light-weight robots, able to work in close contact to humans, that will become numerous in the early future (chapter 3).

Image guidance has been obtained using two-dimensional ultrasound, since is widely used in clinical practice. It is not dangerous for the patient, inexpensive, compact and a highly flexible imaging that allows users to study many anatomic structures. The part of the work regarding calibration of the scan plane in respect to a localization sensor, demonstrates that they exist some simple calibration approaches that allow to easily use traditional ultrasound probes to obtain image guidance (chapter 4).

The realized system for ultrasound guided biopsy (paragraph 5.1) in its entirety, with robotic and mixed reality assistance, is very useful to plan the procedure, allowing to verify, before inserting the needle, the anatomical structures involved during the procedure, to change the access point and to choose the best path. The robot allows to obtain the

desired orientation of the needle automatically, but at the same time leaves the clinician the possibility to change its orientation during insertion so that it can be corrected. A very important feature because the ambient is highly dynamic given the presence of deformable tissues. The image guided system has been designed to use it during the execution of a biopsy but it can be equally useful as a training system using a phantom that replicate the human anatomy constructed with an appropriate material with ultrasound responses similar to the human tissue. As navigation system, it is especially useful for less experienced clinicians who have not yet acquired good 3D orientation skills. Inexpert operators are aided by the virtual scene. They clearly understand the direction of movement to perform with the probe to reach the target.

Furthermore, the introduction of robotics and image guided systems in the daily clinical practice, pave the way to obtain other smart functionalities, where the robot can actively assist the surgeon. For example useful future works using the developed platform could be the introduction of virtual fixtures features, anatomy depending, that do not allow the access into forbidden zones, corresponding to surrounding healthy anatomical structures. Virtual fixtures are easy to integrate in the developed cooperative control, it is enough to vary the coefficients k_i of the matrix K of the controller to provide a resistance more or less strong depending on the distance with the forbidden zones.

The use of mixed reality obtained by the fusion of virtual 3D model with the real time US images, facilitate target localization either in the biopsy system and in the navigation system for HIFU treatments(paragraph 5.2). This allows to reduce the times of sittings, to increase the number of possible treatments and to decrease the risk of potential errors. The 3D reconstruction of the anatomical structures is a very useful aid for preoperative treatment planning providing the clinician a complete knowledge of the patient's anatomy. The clinician orientation during the target area localization was enhanced by virtual views that allow inspection of the anatomy from various viewpoints. In particular during

HIFU treatments the mixed reality view is also very useful in approaching the target of the intervention providing the same benefits of a GPS system for car drivers. The clinician can focalize efforts to find the lesion in the restricted are suggested by the navigator. It is particularly useful in case of lesions difficult to visualize in US images.

The results obtained are encouraging. With regard to the navigation system for the HIFU treatment it is necessary a rigorous clinical experimentation to validate system efficacy. After that the using of the proposed system could be quickly introduced in the clinical practice since it do not require hard certification steps, because it do not introduce a complete automation of the treatment, but leave the clinician the final control before to start the burning phase.

Also the system for biopsy leaves the final control to the clinician. In this case, further than the clinical application, many clinical experts, viewing the system at work, suggested to use it as training system to train the percutaneous insertion of needle under US guidance. The system can show how the probe is positioned in respect to the anatomy, which is very useful to acquire spatial orientation. In case of deep difficulties of the novice, the robot can show the right way to perform the operation. Two steps are necessary to realize the training system. At first to replace the industrial robot with a light weight robot certified to operate near persons. Then to buy or to fabricate realistic ultrasound phantoms for target organs.

References

[1] J. Troccaz, "Computer- and robot-assisted medical interventions," in *HANDBOOK OF AUTOMATION*, Springer ed.

[2] R. H. Taylor and D. Stoianovici, "Medical robotics in computer-integrated surgery," *Ieee Transactions on Robotics and Automation,* vol. 19, pp. 765-781, 2003.

[3] R. H. Taylor*, et al.*, "A TELEROBOTIC ASSISTANT FOR LAPAROSCOPIC SURGERY," *Ieee Engineering in Medicine and Biology Magazine,* vol. 14, pp. 279-288, 1995.

[4] P. J. Kelly*, et al.*, "COMPUTER-ASSISTED STEREOTACTIC LASER MICRO-SURGERY FOR THE TREATMENT OF INTRA-CRANICAL NEOPLASMS," *Neurosurgery,* vol. 10, pp. 324-331, 1982.

[5] N. D. Kitchen*, et al.*, "Accuracy in frame-based and frameless stereotaxy," *Stereotactic and Functional Neurosurgery,* vol. 61, pp. 195-206, 1993.

[6] E. Watanabe*, et al.*, "3-DIMENSIONAL DIGITIZER (NEURONAVIGATOR) - NEW EQUIPMENT FOR COMPUTED TOMOGRAPHY-GUIDED STEREOTAXIC SURGERY," *Surgical Neurology,* vol. 27, pp. 543-547, 1987.

[7] H. K. Gumprecht*, et al.*, "BrainLab VectorVision neuronavigation system: Technology and clinical experiences in 131 cases," *Neurosurgery,* vol. 44, pp. 97-104, 1999.

[8] C. Nimsky*, et al.*, "Quantification of, visualization of, and compensation for brain shift using intraoperative magnetic resonance imaging," *Neurosurgery,* vol. 47, pp. 1070-1079, 2000.

[9] C. Nimsky*, et al.*, "Intraoperative compensation for brain shift," *Surgical Neurology,* vol. 56, pp. 357-364, 2001.

[10] S. Kim*, et al.*, "An Assistive Image-Guided Surgical Robot System Using O-Arm Fluoroscopy for Pedicle Screw Insertion: Preliminary and Cadaveric Study," *Neurosurgery,* vol. 67, pp. 1757-1767, 2010.

[11] C. Matula*, et al.*, "Intraoperative computed tomography guided neuronavigation: concepts, efficiency, and work flow," *Comput Aided Surg,* vol. 3, pp. 174-82, 1998.

[12] S. Zausinger*, et al.*, "Intraoperative Computed Tomography With Integrated Navigation System in Spinal Stabilizations," *Spine,* vol. 34, pp. 2919-2926, 2009.

[13] V. M. Tronnier*, et al.*, "Intraoperative diagnostic and interventional magnetic resonance imaging in neurosurgery," *Neurosurgery,* vol. 40, pp. 891-900, 1997.

[14] C. R. Maurer*, et al.*, "Investigation of intraoperative brain deformation using a 1.5-t interventional MR system: Preliminary results," *Ieee Transactions on Medical Imaging,* vol. 17, pp. 817-825, 1998.

[15] T. Akinbiyi*, et al.*, "Dynamic augmented reality for sensory substitution in robot-assisted surgical systems," *Conf Proc IEEE Eng Med Biol Soc,* vol. 1, pp. 567-70, 2006.

[16] W. A. Hall and C. L. Truwit, "Intraoperative Magnetic Resonance Imaging," *Current Medical Imaging Reviews,* vol. 6, pp. 266-272, 2010.

[17] F. A. Jolesz*, et al.*, "Integration of interventional MRI with computer-assisted surgery," *Journal of Magnetic Resonance Imaging,* vol. 13, pp. 69-77, 2001.

[18] V. Seifert*, et al.*, "Open MRI-guided neurosurgery," *Acta Neurochirurgica,* vol. 141, pp. 455-464, 1999.

[19] J. Koivukangas*, et al.*, "ULTRASOUND-CONTROLLED NEURONAVIGATOR-GUIDED BRAIN SURGERY," *Journal of Neurosurgery,* vol. 79, pp. 36-42, 1993.

[20] G. Unsgaard*, et al.*, "Neuronavigation by Intraoperative three-dimensional ultrasound: Initial experience during brain tumor resection," *Neurosurgery,* vol. 50, pp. 804-812, 2002.

[21] C. Freschi*, et al.*, "An Augmented Reality Navigation Guidance for High Intensity Focused Ultrasound Treatment," in *Conf Proc ICABB, International Conference on Applied Bionics and Biomechanics 2010*, Venice, Italy, 2010.

[22] C. Freschi*, et al.*, "Ultrasound guided robotic biopsy using augmented reality and human-robot cooperative control," *Conf Proc IEEE Eng Med Biol Soc,* vol. 2009, pp. 5110-3, 2009.

[23] S. Condino*, et al.*, "Electromagnetic navigation system for endovascular surgery," 2010.

[24] C. Freschi*, et al.*, "Review of da Vinci Manipulator by technological point of view," *Submitted on Surgical Endoscopy and Other Interventional Techniques*
2011.

[25] A. L. Trejos*, et al.*, "Optimizing port placement for robot-assisted minimally invasive cardiac surgery," *Int J Med Robot,* vol. 3, pp. 355-64, Dec 2007.

[26] J. Binder*, et al.*, "Robotic surgery in urology: fact or fantasy?," *BJU Int,* vol. 94, pp. 1183-7, Nov 2004.

[27] G. S. Guthart and J. K. Salisbury, Jr., "The Intuitive[TM] telesurgery system: overview and application," in *Robotics and Automation, 2000. Proceedings. ICRA '00. IEEE International Conference on*, 2000, pp. 618-621 vol.1.

[28] G. H. Ballantyne and F. Moll, "The da Vinci telerobotic surgical system: the virtual operative field and telepresence surgery," *Surg Clin North Am,* vol. 83, pp. 1293-304, vii, Dec 2003.

[29] Y. Munz*, et al.*, "The benefits of stereoscopic vision in robotic-assisted performance on bench models," *Surg Endosc,* vol. 18, pp. 611-6, Apr 2004.

[30] N. Stylopoulos and D. Rattner, "Robotics and ergonomics," *Surgical Clinics of North America,* vol. 83, pp. 1321-+, 2003.

[31] A. Blavier and A. S. Nyssen, "Influence of 2D and 3D view on performance and time estimation in minimal invasive surgery," *Ergonomics,* vol. 52, pp. 1342-9, Nov 2009.

[32] V. Falk*, et al.*, "Influence of three-dimensional vision on surgical telemanipulator performance," *Surg Endosc,* vol. 15, pp. 1282-8, Nov 2001.

[33] A. Blavier*, et al.*, "Impact of 2D and 3D vision on performance of novice subjects using da Vinci robotic system," *Acta Chir Belg,* vol. 106, pp. 662-4, Nov-Dec 2006.

[34] C. A. LaGrange*, et al.*, "Evaluation of three laparoscopic modalities: robotics versus three-dimensional vision laparoscopy versus standard laparoscopy," *J Endourol,* vol. 22, pp. 511-6, Mar 2008.

[35] G. Hubens*, et al.*, "A performance study comparing manual and robotically assisted laparoscopic surgery using the da Vinci system," *Surg Endosc,* vol. 17, pp. 1595-9, Oct 2003.

[36] G. F. Dakin and M. Gagner, "Comparison of laparoscopic skills performance between standard instruments and two surgical robotic systems," *Surg Endosc,* vol. 17, pp. 574-9, Apr 2003.

[37] N. Di Lorenzo*, et al.*, "Robotic systems and surgical education," *JSLS,* vol. 9, pp. 3-12, Jan-Mar 2005.

[38] S. Jacobs*, et al.*, "The impact of haptic learning in telemanipulator-assisted surgery," *Surg Laparosc Endosc Percutan Tech,* vol. 17, pp. 402-6, Oct 2007.

[39] K. Narazaki*, et al.*, "Robotic surgery training and performance: identifying objective variables for quantifying the extent of proficiency," *Surg Endosc,* vol. 20, pp. 96-103, Jan 2006.

[40] T. N. Judkins*, et al.*, "Real-Time Augmented Feedback Benefits Robotic Laparoscopic Training," *Medicine Meets Virtual Reality 14,* vol. 119, pp. 243-248, 2006.

[41] H. C. Lin*, et al.*, "Towards automatic skill evaluation: detection and segmentation of robot-assisted surgical motions," *Comput Aided Surg,* vol. 11, pp. 220-30, Sep 2006.

[42] S. Kaul*, et al.*, "Learning curve using robotic surgery," *Curr Urol Rep,* vol. 7, pp. 125-9, Mar 2006.

[43] J. Hance*, et al.*, "Skills training in telerobotic surgery," *International Journal of Medical Robotics and Computer Assisted Surgery,* vol. 1, pp. 7-12, 2005.

[44] R. Nayyar and N. P. Gupta, "Critical appraisal of technical problems with robotic urological surgery," *BJU Int,* Oct 28 2009.

[45] L. S. Borden, Jr.*, et al.*, "Mechanical failure rate of da Vinci robotic system," *Can J Urol,* vol. 14, pp. 3499-501, Apr 2007.

[46] H. J. Lavery*, et al.*, "Robotic equipment malfunction during robotic prostatectomy: a multi-institutional study," *J Endourol,* vol. 22, pp. 2165-8, Sep 2008.

[47] Y. W. Jung*, et al.*, "Recent advances of robotic surgery and single port laparoscopy in gynecologic oncology," *J Gynecol Oncol,* vol. 20, pp. 137-44, Sep 2009.

[48] P. Iranmanesh*, et al.*, "Set-up and docking of the da Vinci surgical system: prospective analysis of initial experience," *Int J Med Robot,* vol. 6, pp. 57-60, Mar 2010.

[49] G. Tholey*, et al.*, "Force feedback plays a significant role in minimally invasive surgery: results and analysis," *Ann Surg,* vol. 241, pp. 102-9, Jan 2005.

[50] J. Diks*, et al.*, "Suture damage during robot-assisted vascular surgery: is it an issue?," *Surg Laparosc Endosc Percutan Tech,* vol. 17, pp. 524-7, Dec 2007.

[51] M. Kitagawa*, et al.*, "Effect of sensory substitution on suture-manipulation forces for robotic surgical systems," *J Thorac Cardiovasc Surg,* vol. 129, pp. 151-8, Jan 2005.

[52] D. Ricchiuti*, et al.*, "Diminished Suture Strength After Robotic Needle Driver Manipulation," *J Endourol,* Jul 23 2010.

[53] A. A. Thakre*, et al.*, "Is smaller workspace a limitation for robot performance in laparoscopy?," *J Urol,* vol. 179, pp. 1138-42; discussion 1142-3, Mar 2008.

[54] M. O. Culjat*, et al.*, "A tactile feedback system for robotic surgery," *Conf Proc IEEE Eng Med Biol Soc,* vol. 2008, pp. 1930-4, 2008.

[55] S. D. Herrell*, et al.*, "Toward image guided robotic surgery: system validation," *J Urol,* vol. 181, pp. 783-9; discussion 789-90, Feb 2009.

[56] E. Coste-Maniere*, et al.*, "Planning, simulation, and augmented reality for robotic cardiac procedures: The STARS system of the ChIR team," *Semin Thorac Cardiovasc Surg,* vol. 15, pp. 141-56, Apr 2003.

[57] P. A. Kenney*, et al.*, "Face, content, and construct validity of dV-trainer, a novel virtual reality simulator for robotic surgery," *Urology,* vol. 73, pp. 1288-92, Jun 2009.

[58] G. W. Taylor and D. G. Jayne, "Robotic applications in abdominal surgery: their limitations and future developments," *Int J Med Robot,* vol. 3, pp. 3-9, Mar 2007.

[59] B. C. Shah*, et al.*, "Miniature in vivo robotics and novel robotic surgical platforms," *Urol Clin North Am,* vol. 36, pp. 251-63, x, May 2009.

[60] A. C. Lehman*, et al.*, "Surgery with cooperative robots," *Comput Aided Surg,* vol. 13, pp. 95-105, Mar 2008.

[61] Y. C. Shiu and S. Ahmad, "CALIBRATION OF WRIST-MOUNTED ROBOTIC SENSORS BY SOLVING HOMOGENEOUS TRANSFORM EQUATIONS OF THE FORM AX = XB," *Ieee Transactions on Robotics and Automation,* vol. 5, pp. 16-29, 1989.

[62] R. Y. Tsai and R. K. Lenz, "A NEW TECHNIQUE FOR FULLY AUTONOMOUS AND EFFICIENT 3D ROBOTICS HAND EYE CALIBRATION," *Ieee Transactions on Robotics and Automation,* vol. 5, pp. 345-358, 1989.

[63] H. Q. Zhuang*, et al.*, "SIMULTANEOUS CALIBRATION OF A ROBOT AND A HAND-MOUNTED CAMERA," *Ieee Transactions on Robotics and Automation,* vol. 11, pp. 649-660, 1995.

[64] J. C. K. Chou and M. Kamel, "FINDING THE POSITION AND ORIENTATION OF A SENSOR ON A ROBOT MANIPULATOR USING

QUATERNIONS," *International Journal of Robotics Research,* vol. 10, pp. 240-254, 1991.

[65] F. C. Park and B. J. Martin, "ROBOT SENSOR CALIBRATION - SOLVING AX=XB ON THE EUCLIDEAN GROUP," *Ieee Transactions on Robotics and Automation,* vol. 10, pp. 717-721, 1994.

[66] H. Q. Zhuang and Y. C. Shiu, "A NOISE-TOLERANT ALGORITHM FOR ROBOTIC HAND EYE CALIBRATION WITH OR WITHOUT SENSOR ORIENTATION MEASUREMENT," *Ieee Transactions on Systems Man and Cybernetics,* vol. 23, pp. 1168-1174, 1993.

[67] I. Fassi and G. Legnani, "Hand to sensor calibration: A geometrical interpretation of the matrix equation AX=XB," *Journal of Robotic Systems,* vol. 22, pp. 497-506, 2005.

[68] K. Daniilidis, "Hand-eye calibration using dual quaternions," *International Journal of Robotics Research,* vol. 18, pp. 286-298, 1999.

[69] F. Dornaika and R. Horaud, "Simultaneous robot-world and hand-eye calibration," *Ieee Transactions on Robotics and Automation,* vol. 14, pp. 617-622, 1998.

[70] L. Mercier*, et al.*, "A review of calibration techniques for freehand 3-D ultrasound systems," *Ultrasound in Medicine and Biology,* vol. 31, pp. 143-165, 2005.

[71] J. M. Blackall*, et al.*, "An image registration approach to automated calibration for freehand 3D ultrasound," *Medical Image Computing and Computer-Assisted Intervention - Miccai 2000,* vol. 1935, pp. 462-471, 2000.

[72] E. M. Boctor*, et al.*, "Bootstrapped Ultrasound Calibration," *Medicine Meets Virtual Reality 14,* vol. 119, pp. 61-66, 2006.

[73] L. G. Bouchet*, et al.*, "Calibration of three-dimensional ultrasound images for image-guided radiation therapy," *Physics in Medicine and Biology,* vol. 46, pp. 559-577, 2001.

[74] R. M. Comeau*, et al.*, "Intraoperative ultrasound for guidance and tissue shift correction in image-guided neurosurgery," *Medical Physics,* vol. 27, pp. 787-800, 2000.

[75] S. Dandekar*, et al.*, "A phantom with reduced complexity for spatial 3-D ultrasound calibration," *Ultrasound in Medicine and Biology,* vol. 31, pp. 1083-1093, 2005.

[76] P. R. Detmer*, et al.*, "3D ULTRASONIC IMAGE FEATURE LOCALIZATION BASED ON MAGNETIC SCANHEAD TRACKING - IN-VITRO CALIBRATION AND VALIDATION," *Ultrasound in Medicine and Biology,* vol. 20, pp. 923-936, 1994.

[77] A. H. Gee*, et al.*, "A mechanical instrument for 3D ultrasound probe calibration," *Ultrasound in Medicine and Biology,* vol. 31, pp. 505-518, 2005.

[78] P. W. Hsu*, et al.*, "Rapid, easy and reliable calibration for freehand 3D ultrasound," *Ultrasound in Medicine and Biology,* vol. 32, pp. 823-835, 2006.

[79] P. W. Hsu*, et al.*, "COMPARISON OF FREEHAND 3-D ULTRASOUND CALIBRATION TECHNIQUES USING A STYLUS," *Ultrasound in Medicine and Biology,* vol. 34, pp. 1610-1621, 2008.

[80] A. Khamene and F. Sauer, "A novel phantom-less spatial and temporal ultrasound calibration method," *Medical Image Computing and Computer-Assisted Intervention - Miccai 2005, Pt 2,* vol. 3750, pp. 65-72, 2005.

[81] D. F. Leotta, "An efficient calibration method for freehand 3-D ultrasound imaging systems," *Ultrasound in Medicine and Biology,* vol. 30, pp. 999-1008, 2004.

[82] F. Lindseth*, et al.*, "Probe calibration for freehand 3-D ultrasound," *Ultrasound in Medicine and Biology,* vol. 29, pp. 1607-1623, 2003.

[83] D. M. Muratore and R. L. Galloway, "Beam calibration without a phantom for creating a 3-D freehand ultrasound system," *Ultrasound in Medicine and Biology,* vol. 27, pp. 1557-1566, 2001.

[84] N. Pagoulatos*, et al.*, "A fast calibration method for 3-D tracking of ultrasound images using a spatial localizer," *Ultrasound in Medicine and Biology,* vol. 27, pp. 1219-1229, 2001.

[85] R. W. Prager*, et al.*, "Rapid calibration for 3-D freehand ultrasound," *Ultrasound in Medicine and Biology,* vol. 24, pp. 855-869, 1998.

[86] State A*, et al.*, "Case study: Observing a volume rendered fetus within a pregnant patient," presented at the IEEE Conference on Visualization, 1994.

[87] D. C. Barratt*, et al.*, "Self-calibrating 3D-ultrasound-based bone registration for minimally invasive orthopedic surgery," *Ieee Transactions on Medical Imaging,* vol. 25, pp. 312-323, 2006.

[88] A. Krupa and F. Chaumette, "Guidance of an ultrasound probe by visual servoing," *Advanced Robotics,* vol. 20, pp. 1203-1218, 2006.

[89] J. Moré, "The Levenberg-Marquardt algorithm: Implementation and theory " *Numerical Analysis*
Lecture Notes in Mathematics, vol. - 630, pp. - 116, 1978.

[90] O. Péria*, et al.*, "Using a 3D position sensor for registration of SPECT and US images of the kidney," *Computer Vision, Virtual Reality and Robotics in Medicine*
Lecture Notes in Computer Science, vol. - 905, pp. - 29, 1995.

[91] F. Rousseau*, et al.*, "Quantitative evaluation of three calibration methods for 3-D freehand ultrasound," *Ieee Transactions on Medical Imaging,* vol. 25, pp. 1492-1501, 2006.

[92] M. Baumann*, et al.*, "3-D ultrasound probe calibration for computer-guided diagnosis and therapy," *Computer Vision Approaches to Medical Image Analysis,* vol. 4241, pp. 248-259, 2006.

[93] T. Lango, "Ultrasound guided surgery: image processing and navigation," Norwegian University of Science and Technology, Trondheim,
Norwa, 2000.

[94] A. Ali and R. Logeswaran, "A visual probe localization and calibration system for cost-effective computer-aided 3D

ultrasound," *Computers in Biology and Medicine,* vol. 37, pp. 1141-1147, 2007.

[95] J. Varandas*, et al.*, "VOLUS - a visualization system for 3D ultrasound data," *Ultrasonics,* vol. 42, pp. 689-694, 2004.

[96] Y. Sato*, et al.*, "Image guidance of breast cancer surgery using 3-D ultrasound images and augmented reality visualization," *Ieee Transactions on Medical Imaging,* vol. 17, pp. 681-693, 1998.

[97] W. Y. Zhang*, et al.*, "Freehand 3D ultrasound calibration using an electromagnerically tracked needle," in *Medical Imaging : Visualization, Image-Guided Procedures, and Display*, 2006.

[98] J. N. Welch*, et al.*, "A real-time freehand 3D ultrasound system for image-guided surgery," *IEEE Ultrasonics Symposium,* 2000.

[99] R. Beasley*, et al.*, "Registration of Ultrasound Images," in *Proceedings of the SPIE - The International Society for Optical Engineering*, 1999.

[100] E. M. Boctor*, et al.*, "A rapid calibration method for registration and 3d tracking of ultrasound images using spatial localizer," in *Proc. SPIE*, 2003.

[101] A. Viswanathan*, et al.*, "Immediate ultrasound calibration with three poses and minimal image processing," *Medical Image Computing and Computer-Assisted Intervention - Miccai 2004, Pt 2, Proceedings,* vol. 3217, pp. 446-454, 2004.

[102] R. Alterovitz*, et al.*, "Planning for Steerable Bevel-tip Needle Insertion Through 2D Soft Tissue with Obstacles," 2005.

[103] S. DiMaio and S. Salcudean, "Needle Steering and Model-Based Trajectory Planning," in *Miccai*, 2003.

[104] E. M. Boctor*, et al.*, "Virtual remote center of motion control for needle placement robots," *Comput Aided Surg,* vol. 9, pp. 175-83, 2004.

[105] L. Zhang*, et al.*, "High-intensity focused ultrasound (HIFU): effective and safe therapy for hepatocellular carcinoma adjacent to major hepatic veins," *European Radiology,* vol. 19, pp. 437-445, 2009.

[106] J. E. Kennedy, "High-intensity focused ultrasound in the treatment of solid tumours," *Nature Reviews Cancer,* vol. 5, pp. 321-327, 2005.

[107] F. Wu*, et al.*, "Extracorporeal focused ultrasound surgery for treatment of human solid carcinomas: Early Chinese clinical experience," *Ultrasound in Medicine and Biology,* vol. 30, pp. 245-260, 2004.

[108] T. Klatte and M. Marberger, "High-intensity focused ultrasound for the treatment of renal masses: current status and future potential," *Current Opinion in Urology,* vol. 19, pp. 188-191, 2009.

[109] X. L. Ren*, et al.*, "Sonographically Guided Extracorporeal Ablation of Uterine Fibroids With High-Intensity Focused Ultrasound: Midterm Results," *Journal of Ultrasound in Medicine,* vol. 28, pp. 100-103, 2009.

[110] T. J. Dubinsky*, et al.*, "High-intensity focused ultrasound: Current potential and oncologic applications," *American Journal of Roentgenology,* vol. 190, pp. 191-199, 2008.

[111] L. Crocetti*, et al.*, "Targeting liver lesions for radipfrequency ablation - An experimental feasibility study using a CT-US fusion imaging system," *Investigative Radiology,* vol. 43, pp. 33-39, 2008.